

# Monometallic and bimetallic titanium $\kappa^1$ -amidinate complexes as olefin polymerization catalysts

Richard A. Collins<sup>a</sup>, Adam F. Russell<sup>a</sup>, Richard T. W. Scott<sup>a,b</sup>, Raffaele Bernardo<sup>b</sup>, Gerard H. J. van Doremaele,<sup>b</sup> Alexandra Berthoud<sup>\*b</sup> and Philip Mountford<sup>\*a</sup>

(a) Chemistry Research Laboratory, Department of Chemistry, University of Oxford, Mansfield Road, Oxford OX1 3TA, UK.

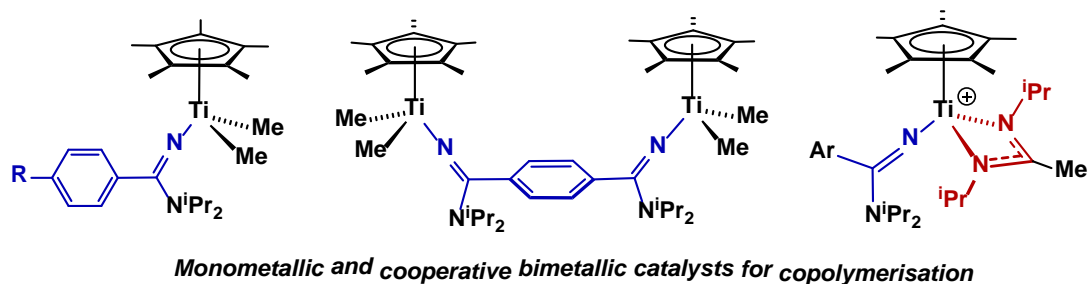
(b) Arlanxeo Netherlands B.V., Urmonderbaan 24, 6167 RD GELEEN, The Netherlands.

Email: philip.mountford@chem.ox.ac.uk or alexandra.berthoud@ARLANXEO.com

## Abstract

A series of cyclopentadienyl- $\kappa^1$ -amidinate titanium complexes  $\text{Cp}^*\text{Ti}\{\text{NC}(\text{Ar}^R)\text{N}^i\text{Pr}_2\}\text{Me}_2$  ( $\text{Ar}^R = 4\text{-C}_6\text{H}_4\text{R}$  where  $\text{R} = \text{H}$  (**1-Me**),  $\text{CF}_3$  (**5-Me**),  $^i\text{Bu}$  (**6-Me**) and  $\text{NMe}_2$  (**7-Me**)) with different *para*-substituents in the amidinate ligand were synthesised and structurally characterised, along with three bimetallic analogues:  $1,4\text{-C}_6\text{H}_4\{\text{C}(\text{N}^i\text{Pr}_2)\text{N}\}_2\{\text{Cp}^*\text{TiMe}_2\}_2$  (**2-Me**),  $1,3\text{-C}_6\text{H}_4\{\text{C}(\text{N}^i\text{Pr}_2)\text{N}\}_2\{\text{Cp}^*\text{TiMe}_2\}_2$  (**3-Me**) and  $\text{CH}_2\{1,4\text{-C}_6\text{H}_4\text{-C}(\text{N}^i\text{Pr}_2)\text{N}\}_2\{\text{Cp}^*\text{TiMe}_2\}_2$  (**4-Me**).  $^{13}\text{C}$  NMR spectroscopy, density function theory (DFT) and the quantum theory of atoms-in-molecules (QTAIM) were used to evaluate the donor ability of the various  $\text{NC}(\text{Ar}^R)\text{N}^i\text{Pr}_2$  ligands and the influence of the  $\text{Ar}^R$  group *para*-substituents. Reaction of **1-Me** and certain homologues, as well as of **2-Me**, with borate and borane reagents  $[\text{CPh}_3][\text{B}(\text{Ar}^{\text{F}_5})_4]$  ( $\text{Ar}^{\text{F}_5} = \text{C}_6\text{F}_5$ ),  $\text{B}(\text{Ar}^{\text{F}_5})_3$ , in the absence or presence of Lewis bases or polar unsaturated substrates were carried out, forming adducts and migratory insertion products such as  $[\text{Cp}^*\text{Ti}\{\text{NC}(\text{Ph})\text{N}^i\text{Pr}_2\}\text{Me}(\text{THF})][\text{BF}_{20}]$ ,  $[\text{Cp}^*\text{Ti}\{\text{NC}(\text{Ph})\text{N}^i\text{Pr}_2\}\{\text{MeC}(\text{N}^i\text{Pr})_2\}][\text{BF}_{20}]$  and  $[1,4\text{-C}_6\text{H}_4\{\text{C}(\text{N}^i\text{Pr}_2)\text{N}\}_2\{\text{Cp}^*\text{Ti}\{\text{MeC}(\text{N}^i\text{Pr})_2\}_2\}][\text{BF}_{20}]_2$ . Detailed olefin co-polymerization studies for forming EPDM from ethylene, propylene and certain dienes were carried out with mono- and bi-metallic catalysts and borate and borane activators. Catalyst-activator effects on polymerization productivity and polymer composition relationships were mapped out. The bimetallic catalysts **2** and **3** showed cooperative effects based on electronic factors leading to enhanced propene incorporation but unfavorable steric effects gave lower diene content. Related but less significant electronic effects on propene affinity were found for the monometallic catalysts  $\text{Cp}^*\text{Ti}\{\text{NC}(\text{Ar}^R)\text{N}^i\text{Pr}_2\}\text{Me}_2$  as the  $\text{Ar}^R$  moiety *para*-substituents were varied.

## TOC graphic



## Introduction

Homogeneous olefin polymerization catalysis continues to be an area of considerable importance to both the academic and industrial communities, and a wide range of cyclopentadienyl and non-cyclopentadienyl based transition metal systems have been described.<sup>1</sup> With specific regard to the Group 4 metals, the spectacular success of metallocene systems as single-site olefin polymerization catalysts<sup>2</sup> was followed by the development of a range of half-sandwich compounds, starting with the cyclopentadienyl-amido “constrained geometry catalysts” (CGCs)<sup>3</sup> and then other systems<sup>4</sup> of the type  $(\eta\text{-C}_5\text{R}_5)\text{M}(\text{X})\text{R}_2$  in which the ‘X’ ligand is a heteroatom-donor moiety such as aryloxide (OAr),<sup>4-5</sup> phosphinimide ( $\text{NPR}_3$ ),<sup>6</sup> cyclic or non-cyclic guanidine( $\text{NC}(\text{NR}_2)_2$ ),<sup>7</sup> ketimide ( $\text{NCR}_2$ )<sup>8</sup> or  $\kappa^1$ -benzamidinate ( $\text{NC}(\text{Ar})\text{NR}_2$ ).<sup>9</sup> Non-cyclopentadienyl systems were also developed featuring bis(amide)-type ligands<sup>10</sup> and their bis(phenoxy) and related analogues,<sup>11</sup> typically incorporating additional Lewis base donors. Catalyst systems based on imido ligands with additional *fac*-N<sub>3</sub> donor ligand sets were also developed,<sup>12</sup> building on and exploiting the isolobal analogy between cyclopentadienide and these N-donor ligand sets.<sup>13</sup>

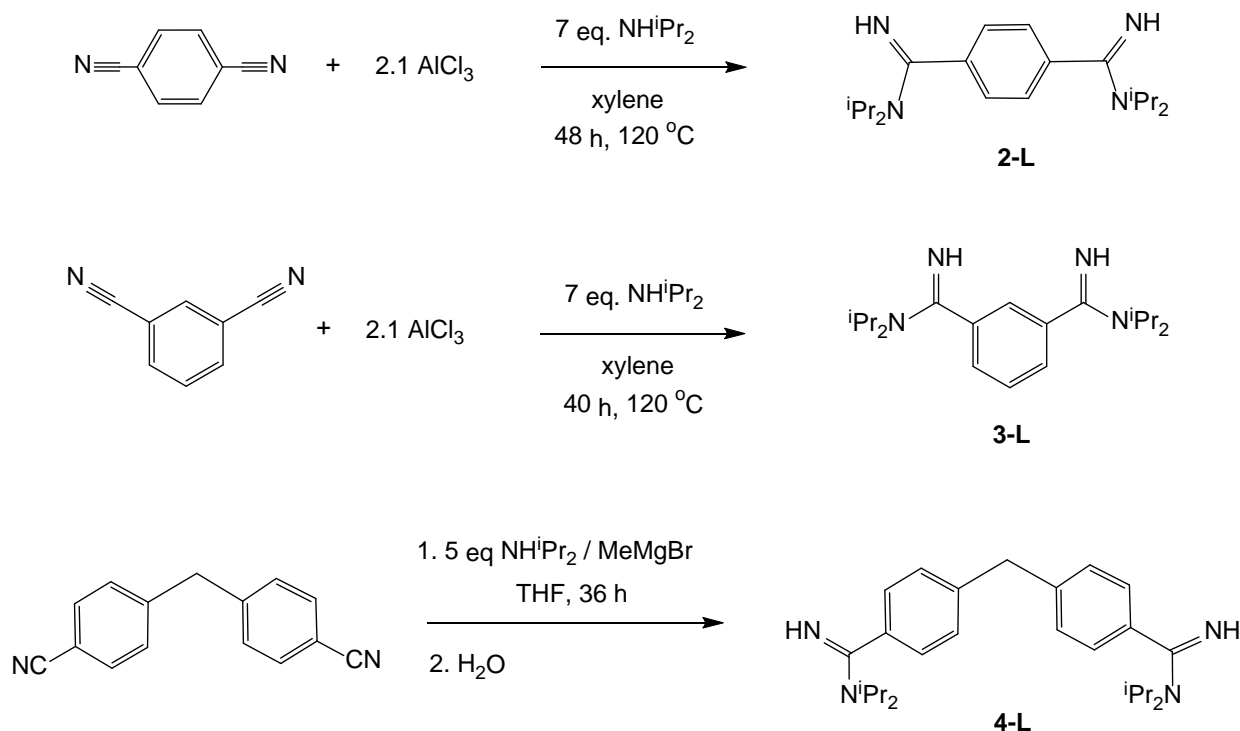
In addition to these first-developed monometallic catalysts, bimetallic systems containing metal centers either tethered covalently through sophisticated ligand design, or brought together in a template-type manner using a binuclear cocatalyst (i.e. a bis(borane) or bis(borate) species), have been reported in the last 10-15 years as delivering beneficial cooperative effects in olefin polymerization.<sup>14</sup> Metallocene, half-sandwich and non-cyclopentadienyl systems have all been studied. Although not all bimetallic systems show strong (or indeed any) improvements, enhancements to molecular weight capacity,<sup>15</sup> chain branching<sup>15a, 16</sup> and degree of  $\alpha$ -olefin enchainment<sup>15b, 16-17</sup> as well stereo- and regio-chemistry<sup>15c, 18</sup> have all been demonstrated. These effects have been attributed to (in certain cases with computational support<sup>19</sup>) to secondary interactions from a proximate metal centre acting on either a growing polymeryl chain, monomer unit or terminated polymer chain.

Arlanxeo<sup>20</sup> has developed (as Keltan ACE<sup>TM</sup>)<sup>21</sup> a class of half-sandwich  $\kappa^1$ -amidinate titanium complexes of the type  $(\eta\text{-C}_5\text{R}_5)\text{Ti}\{\text{NC}(\text{Ar})\text{NR}'_2\}\text{X}_2$  ( $\text{X} = \text{Me}$  or  $\text{Cl}$ ), which are extremely active pre-catalysts for the commercial homo- and co-polymerization of olefins.<sup>9a-c</sup> In a preliminary communication we reported the synthesis and activation chemistry of  $\text{Cp}^*\text{Ti}\{\text{NC}(\text{Ar}^{\text{F}2})\text{N}^i\text{Pr}_2\}\text{Me}_2$  ( $\text{Ar}^{\text{F}2} = \text{C}_6\text{H}_3\text{F}_2$  (**9-Me**)) and some preliminary results regarding the copolymerization of ethylene and propylene.<sup>9d</sup> Here we expand on this preliminary communication with a series of mono- and bi-metallic complexes, their activation chemistry and olefin polymerization performance using borate and other activators, together with DFT studies.

## Results and discussion

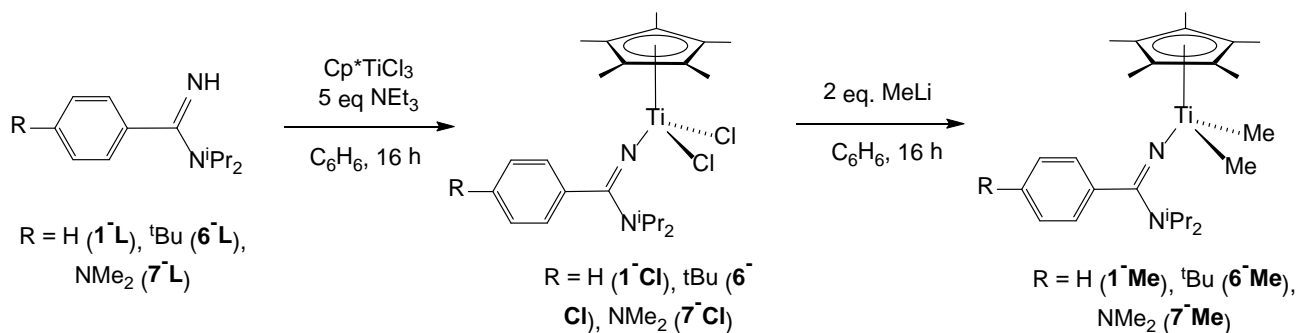
### Synthesis and characterization of monometallic and bimetallic $\kappa^1$ -amidinate titanium complexes

*Ligand synthesis.* The neutral benzamidine  $\text{HNC}(\text{Ph})\text{N}^i\text{Pr}_2$  (**1-L**) was synthesised as a ligand precursor by nucleophilic attack on the nitrile group of  $\text{PhCN}$  by the *in situ* generated magnesium amide,  $^i\text{Pr}_2\text{NMgBr}$ , followed by quenching with methanol and water. The same method was initially used to synthesise three new bis(amidine) compounds: 1,4- $\text{C}_6\text{H}_4\{\text{C}(\text{N}^i\text{Pr}_2)\text{NH}\}_2$  (**2-L**), 1,3- $\text{C}_6\text{H}_4\{\text{C}(\text{N}^i\text{Pr}_2)\text{NH}\}_2$  (**3-L**) and the unconjugated variant  $\text{CH}_2\{1,4\text{-C}_6\text{H}_4\text{-C}(\text{N}^i\text{Pr}_2)\text{NH}\}_2$  (**4-L**). Unlike their mono-substituted and non-conjugated counterparts (e.g. **4-L**), very forcing conditions were required for both **2-L** and **3-L**, leading to low yields (34-38%). A large excess of the *in situ* generated Grignard reagent,  $^i\text{Pr}_2\text{NMgBr}$  and additionally, in the case of **3-L**, a prolonged reaction time (24 h) under reflux conditions were required. This is likely a result of the difficulty in a nucleophilic attack on a nitrile conjugated to a deprotonated amidine. However, using  $\text{AlCl}_3$  in the presence of an excess of diisopropylamine at high temperatures (120 °C) in a minimum amount of xylene proved to be higher yielding for **2-L** and **3-L** (86 and 80%, respectively). The synthetic routes are summarized in Scheme 1. The synthesis of 1,2- $\text{C}_6\text{H}_4\{\text{C}(\text{N}^i\text{Pr}_2)\text{NH}\}_2$  was not attempted due to the facile formation of phthalocyanines from the required precursors.



**Scheme 1.** Synthesis of new bis(amidine) compounds

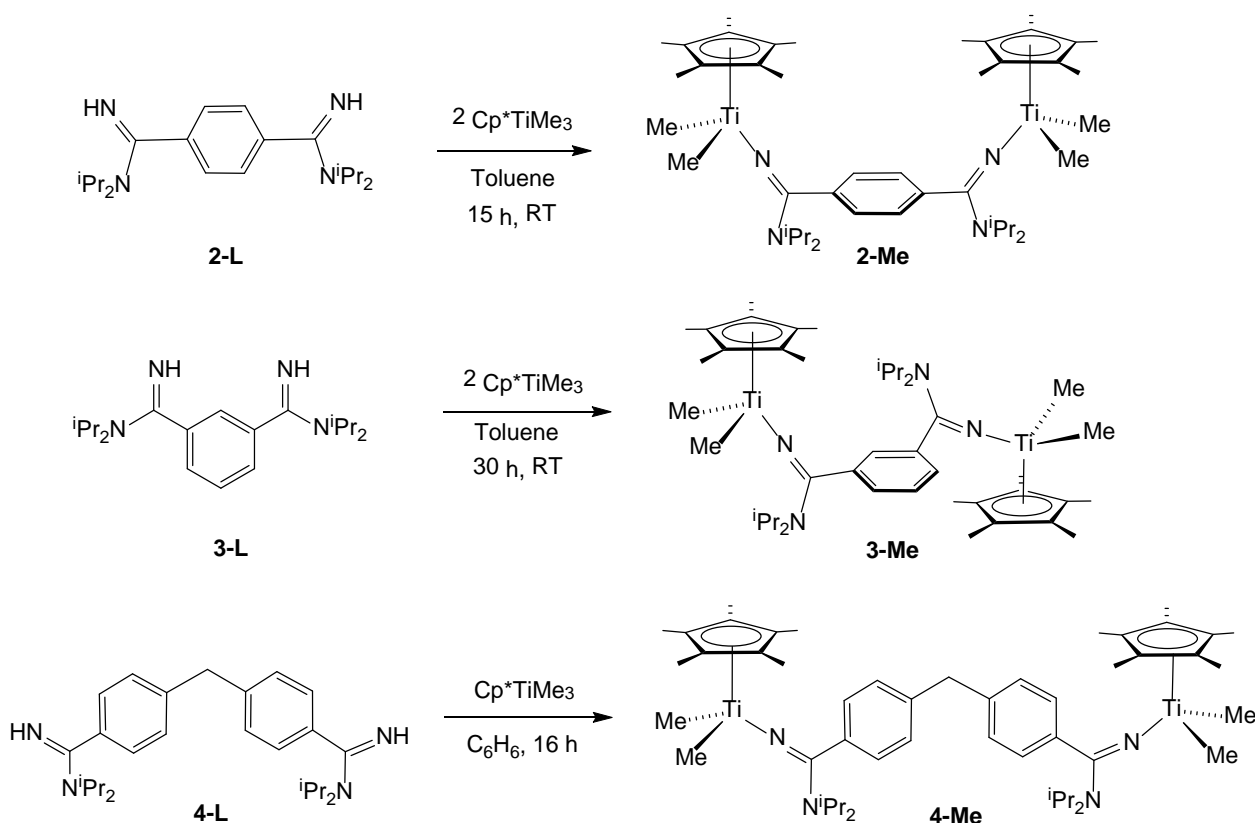
*Synthesis of titanium complexes.* The monometallic dichloride  $\text{Cp}^*\text{Ti}\{\text{NC}(\text{Ph})\text{N}^i\text{Pr}_2\}\text{Cl}_2$  (**1-Cl**) was prepared in 54% yield by reaction of  $\text{HNC}(\text{Ph})\text{N}^i\text{Pr}_2$  (**1-L**) with  $\text{Cp}^*\text{TiCl}_3$  in the presence of an excess of triethylamine (Scheme 2). Methylation of **1-Cl** with 2 equivalents of  $\text{MeLi}$  proceeded smoothly to give  $\text{Cp}^*\text{Ti}\{\text{NC}(\text{Ph})\text{N}^i\text{Pr}_2\}\text{Me}_2$  (**1-Me**) in 40% isolated yield following recrystallization from hexane.



**Scheme 2.** Synthesis of monometallic  $\kappa^1$ -amidinate titanium compounds.

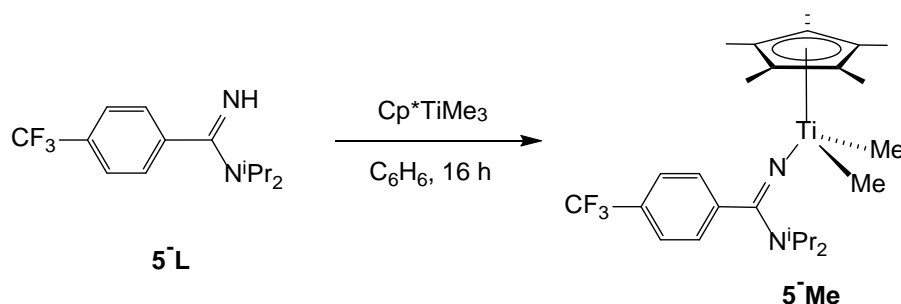
An NMR tube scale experiment showed that **1-Me** could alternatively be prepared from  $\text{Cp}^*\text{TiMe}_3$  and 1 equiv of **1-L**. This protonolysis pathway was employed for the synthesis of 1,4- $\text{C}_6\text{H}_4\{\text{C}(\text{N}^i\text{Pr}_2)\text{N}\}_2\{\text{Cp}^*\text{TiMe}_2\}_2$  (**2-Me**), 1,3- $\text{C}_6\text{H}_4\{\text{C}(\text{N}^i\text{Pr}_2)\text{N}\}_2\{\text{Cp}^*\text{TiMe}_2\}_2$  (**3-Me**) and  $\text{CH}_2\{1,4\text{-C}_6\text{H}_4\text{-C}(\text{N}^i\text{Pr}_2)\text{N}\}_2\{\text{Cp}^*\text{TiMe}_2\}_2$  (**4-Me**) from the respective bis(amidine) in 51, 46 and 48% isolated yields, respectively (Scheme 3). The new compounds **1-Cl**, **1-Me**, **2-Me**, **3-Me** and **4-Me** were fully characterised by standard spectroscopic and analytic techniques (see the Supporting Information).

The  $^1\text{H}$  NMR spectra (298 K,  $\text{C}_6\text{D}_6$ ) of **1-Cl**, **1-Me**, **2-Me**, **3-Me** and **4-Me** indicate  $C_s$ -symmetry on the NMR timescale. Broad resonances are observed for the isopropyl groups as a result of restricted rotation about the  $\text{C}-\text{N}^i\text{Pr}_2$  bond. At low temperature the *isopropyl* group signals resolve into two doublets and two septets in the case of **1-Cl**, **1-Me**, **2-Me** and **4-Me**. The planar chirality of **3-Me** results in all four methyl groups of  $-\text{N}^i\text{Pr}_2$  becoming inequivalent, and the  $\text{TiMe}_2$  signal decoalesces into 2 resonances. For the same amidinate ligand it is invariably found that the barrier to rotation about the  $\text{C}-\text{N}^i\text{Pr}_2$  bond is lower for the titanium dimethyl complexes than the dichloride ones, consistent with the structural data reported later (longer  $\text{C}-\text{N}^i\text{Pr}_2$  and shorter  $\text{C}=\text{N}-\text{Ti}$  bonds for the dimethyl complexes).



**Scheme 3.** Synthesis of new bimetallic  $\kappa^1$ -amidinate titanium compounds.

A further series of *para*-substituted benzamidinate complexes  $\text{Cp}^*\text{Ti}\{\text{NC}(\text{Ar}^R)\text{N}^i\text{Pr}_2\}\text{Me}_2$  ( $\text{Ar}^R = 4\text{-C}_6\text{H}_4\text{R}$ ,  $\text{R} = \text{CF}_3$  (**5-Me**),  $^t\text{Bu}$  (**6-Me**) or  $\text{NMe}_2$  (**7-Me**)) were also synthesised. These were prepared either directly or indirectly from the corresponding neutral analogues of **1-L**, namely **5-L**, **6-L** and **7-L**. The benzamidines themselves were obtained in 55 – 84% yield by an analogous route to that used for **1-L** (see the SI).<sup>22</sup>



**Equation 1**

A protonolysis reaction between  $\text{HNC}(\text{Ar}^{\text{CF}_3})\text{N}^i\text{Pr}_2$  (**5-L**) and  $\text{Cp}^*\text{TiMe}_3$  proved facile and generated  $\text{Cp}^*\text{Ti}\{\text{NC}(\text{Ar}^{\text{CF}_3})\text{N}^i\text{Pr}_2\}\text{Me}_2$  (**5-Me**) in good yield at room temperature within 17 h (Eq. 1). The analogous reactions of  $\text{Cp}^*\text{TiMe}_3$  with  $\text{HNC}(\text{Ar}^{\text{tBu}})\text{N}^i\text{Pr}_2$  (**6-L**) or  $\text{HNC}(\text{Ar}^{\text{NMe}_2})\text{N}^i\text{Pr}_2$  (**7-L**) were unsuccessful even at elevated temperatures. This reduced reactivity apparently results from the more electron-donating  $^t\text{Bu}$  and  $\text{NMe}_2$  *para*-substituents of **6-L** and **7-L** decreasing the acidity of the amidine (the Hammett  $\sigma_p$  values are 0.54, -0.20 and -0.83 for  $\text{CF}_3$ ,  $^t\text{Bu}$  and  $\text{NMe}_2$ , respectively, with  $\sigma_p$  for H being defined as 0.0).<sup>23</sup> Fortunately, reaction of **6-L** or **7-L** with  $\text{Cp}^*\text{TiCl}_3$  in the presence of an excess of triethylamine gave the dichloride complexes,  $\text{Cp}^*\text{Ti}\{\text{NC}(\text{Ar}^{\text{tBu}})\text{N}^i\text{Pr}_2\}\text{Cl}_2$  (**6-Cl**) and  $\text{Cp}^*\text{Ti}\{\text{NC}(\text{Ar}^{\text{NMe}_2})\text{N}^i\text{Pr}_2\}\text{Cl}_2$  (**7-Cl**) in 48 and 79% yields, respectively (Scheme 2). Subsequent reaction with 2 equivalents of  $\text{MeLi}$  gave the target dimethyl compounds  $\text{Cp}^*\text{Ti}\{\text{NC}(\text{Ar}^{\text{tBu}})\text{N}^i\text{Pr}_2\}\text{Me}_2$  (**6-Me**) and  $\text{Cp}^*\text{Ti}\{\text{NC}(\text{Ar}^{\text{NMe}_2})\text{N}^i\text{Pr}_2\}\text{Me}_2$  (**7-Me**). The  $^1\text{H}$  and  $^{13}\text{C}$  NMR spectra of compounds **5-Me**, **6-Me** and **7-Me** were generally comparable to those of **1-Me** and to each other.

In addition to the amidinate complexes so far mentioned (and their ligand precursors) with neutral *para*-substituents, we attempted to prepare complexes of the type  $[\text{Cp}^*\text{Ti}\{\text{NC}(\text{Ar}^{\text{R}^+})\text{N}^i\text{Pr}_2\}\text{X}_2][\text{BF}_2\text{O}]$  ( $\text{X} = \text{Cl}$  or  $\text{Me}$ ;  $[\text{BF}_2\text{O}]^- = [\text{B}(\text{Ar}^{\text{F}_5})_4]^-$  ( $\text{Ar}^{\text{F}_5} = \text{C}_6\text{F}_5$ );  $\text{Ar}^{\text{R}^+} = 4\text{-C}_6\text{H}_4\text{NMe}_3$ ) as a better mimic of the electronic effects of a distal cationic metal center in the activate bimetallic polymerization catalysts. Unfortunately, these attempts were all unsuccessful. Further details are given in the SI.

*Solid state structures of neutral benzamidines.* The neutral amidines **1-L**, **2-L**, **3-L** and **5-L** have all been crystallographically characterised. The structures and selected bond lengths and angles are given in Fig. S1 and Table S1 of the Supporting Information. The molecular structure of **1-L** is shown by way of example in Fig. 1. The bond lengths and angles are all within the usual ranges,<sup>24</sup> and there are no significant differences between any of the structures, despite the differences in *para*-substituents. In all cases the phenyl ring lies approximately perpendicular to  $\text{N}(1)=\text{C}(1)-\text{N}(2)^i\text{Pr}_2$  plane, presumably to avoid unfavourable steric interactions. Therefore there is little or no  $\pi$ -conjugation between the  $4\text{-C}_6\text{H}_4\text{R}$  ring and the  $-\text{C}(\text{N}^i\text{Pr}_2)=\text{N}-\text{Ti}$  linkage.

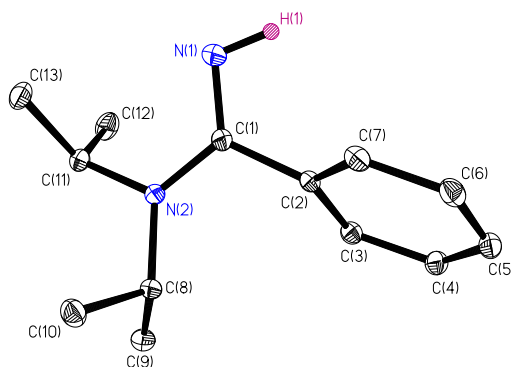


**Figure 1.** Displacement ellipsoid plot (20% probability) of HNC(Ph)N<sup>i</sup>Pr<sub>2</sub> (**1-L**). C-bound H atoms omitted.

*Solid state structures of the dichloride complexes.* Diffraction-quality crystals of the dichlorides Cp<sup>\*</sup>Ti{NC(Ph)N<sup>i</sup>Pr<sub>2</sub>}Cl<sub>2</sub> (**1-Cl**), Cp<sup>\*</sup>Ti{NC(Ar<sup>t</sup>Bu)N<sup>i</sup>Pr<sub>2</sub>}Cl<sub>2</sub> (**6-Cl**) and Cp<sup>\*</sup>Ti{NC(Ar<sup>NMe2</sup>)N<sup>i</sup>Pr<sub>2</sub>}Cl<sub>2</sub> (**7-Cl**) were also obtained. The molecular structure of **6-Cl** is shown by way of example in Fig. 2 and the others are shown in Fig S2 of the SI. Selected bond distances and angles for all three are listed in Table 1.

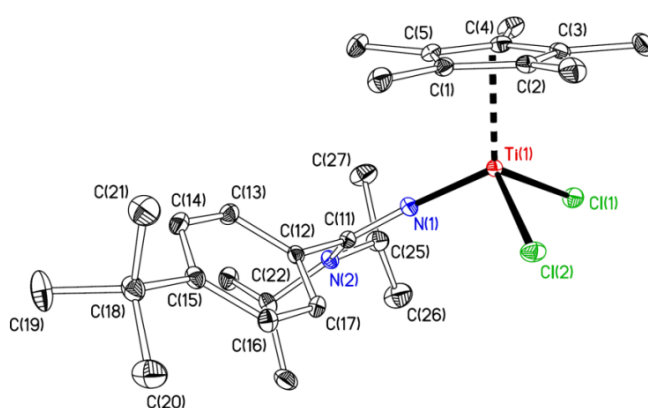


**Figure 2.** Displacement ellipsoid plot of Cp<sup>\*</sup>Ti{NC(Ar<sup>t</sup>Bu)N<sup>i</sup>Pr<sub>2</sub>}Cl<sub>2</sub> (**6-Cl**) (20% probability, C-bound H atoms omitted).

**Table 1.** Selected bond lengths (Å) and angles (°) for Cp\*Ti{NC(Ph)N<sup>i</sup>Pr<sub>2</sub>}Cl<sub>2</sub> (**1-Cl**), Cp\*Ti{NC(Ar<sup>tBu</sup>)N<sup>i</sup>Pr<sub>2</sub>}Cl<sub>2</sub> (**6-Cl**) and Cp\*Ti{NC(Ar<sup>NMe<sub>2</sub></sup>)N<sup>i</sup>Pr<sub>2</sub>}Cl<sub>2</sub> (**7-Cl**). Cp\*<sub>cent</sub> is the computed Cp\* ring carbon centroid.

Parameter	<b>1-Cl</b>	<b>6-Cl</b>	<b>7-Cl</b>
Ti(1)-Cp* <sub>cent</sub>	2.05	2.04	2.05
Ti(1)-N(1)	1.800(3)	1.798(2)	1.792(2)
N(1)-C(11)	1.310(4)	1.302(3)	1.310(2)
N(2)-C(11)	1.340(4)	1.355(3)	1.344(2)
C(11)-C(12)	1.509(5)	1.499(3)	1.499(3)
Ti(1)-Cl(1)	2.3137(11)	2.2965(8)	2.2927(6)
Ti(1)-Cl(2)	2.3051(11)	2.3066(7)	2.3266(6)
Cp* <sub>cent</sub> -Ti(1)-N(1)	118.0	116.0	117.8
Cp* <sub>cent</sub> -Ti(1)-Cl(1)	113.5	115.1	116.2
Cp* <sub>cent</sub> -Ti(1)-Cl(2)	115.0	115.1	112.9
C(11)-N(1)-Ti(1)	165.2(3)	168.25(19)	164.28(14)

All of the complexes have the expected three-legged piano stool arrangement at titanium, and the Ti–Cl and Ti–Cp\* distances lie within the usual ranges. The Ti(1)–N(1) bond lengths (av. 1.796, range 1.7920(17) – 1.800(3) Å) are significantly longer than the typical values for a Ti–N<sub>amide</sub> ( $\sigma^2\pi^2$ ) partial double bond (typically 1.90 - 2.00 Å),<sup>25</sup> and closer to those of Ti≡N ( $\sigma^2\pi^4$ ) triple bonds, such as are found in titanium imido compounds (L)Ti≡NR,<sup>26</sup> which usually lie in the range *ca.* 1.69 – 1.75 Å.<sup>24, 27</sup> They are also all significantly shorter than that in the ketimide analogue Cp\*Ti(NC<sup>t</sup>Bu<sub>2</sub>)Cl<sub>2</sub> (**8**, Ti–N = 1.844(7) Å).<sup>28</sup> These data suggest a Ti–N bonding description in Cp\*Ti{NC(Ar<sup>R</sup>)N<sup>i</sup>Pr<sub>2</sub>}Cl<sub>2</sub> that lies between the two extremes of  $\sigma^2\pi^2$  (amide-like) and  $\sigma^2\pi^4$  (imide-like), such that the donating capacity of the amidinate group is intermediate between the 3- and 5-electron limits (*cf.* resonance forms **A** and **B** in Fig. 3), as has been discussed for the related phosphinimide and cyclic guanidinate counterparts.<sup>6b, 7a</sup> The approximately linear C(11)–N(1)–Ti(1) bond angles (av. 165.9 °, range 164.28(14) – 168.25(19) °) are consistent with effective  $\pi$ -donation from N(1). The N<sup>i</sup>Pr<sub>2</sub> nitrogen N(2) and the central carbon C(11) of the ArC(N)N<sup>i</sup>Pr<sub>2</sub> linkage have approximately trigonal planar geometries, implying  $sp^2$  hybridization, and the N(2)–C(11) and C(11)–N(1) distances (av. 1.346 and 1.307 Å) are shorter and longer, respectively, than in the parent



amidines themselves (av. 1.365 and 1.289 Å, respectively; cf. Fig. S1 and Table S1 of the SI), consistent with a significant contribution from the imide-like resonance form **B** (Fig. 3). The bonding is discussed in further detail below.

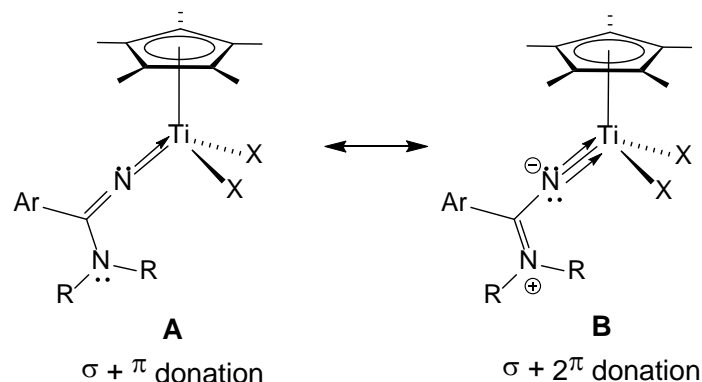


**Figure 3.** Resonance contributions to the Ti–N<sub>amidinate</sub> bonding. **A**: 3-electron donor,  $\sigma^2\pi^2$  Ti–N<sub>amidinate</sub> bond; **B**: 5-electron donor (“imide-like”)  $\sigma+2\pi$  Ti–N<sub>amidinate</sub> bond

In all three complexes, as in the neutral benzamidines themselves, the planes of the aryl ring carbons lie approximately perpendicular to the  $\text{N}(1)=\text{C}(11)-\text{N}(2)^i\text{Pr}_2$  plane (av. rotation out of co-planarity = *ca.*  $65 \pm 10^\circ$ ). As a result, even though the phenyl *para*-substituent varies considerably between the three compounds, there is no statistically significant change trend for any of the key structural parameters. Nonetheless, the Ti(1)–N(1) distance in  $\text{Cp}^*\text{Ti}\{\text{NC}(\text{Ar}^{\text{NMe}_2})\text{N}^i\text{Pr}_2\}\text{Cl}_2$  (**7-Cl**) with the strongest donor *para*-substituent, appears to tend towards the shortest of the three examples.

*Solid state structures of the dimethyl complexes.* Diffraction-quality crystals of the monotitanium dimethyl compounds  $\text{Cp}^*\text{Ti}\{\text{NC}(\text{Ph})\text{N}^i\text{Pr}_2\}\text{Me}_2$  (**1-Me**),  $\text{Cp}^*\text{Ti}\{\text{NC}(\text{Ar}^{\text{tBu}})\text{N}^i\text{Pr}_2\}\text{Me}_2$  (**6-Me**) and  $\text{Cp}^*\text{Ti}\{\text{NC}(\text{Ar}^{\text{NMe}_2})\text{N}^i\text{Pr}_2\}\text{Me}_2$  (**7-Me**) were also obtained. The molecular structure of **1-Me** is shown in Fig. 4 by way of example, and the others are given in Fig. S3 of the SI. Selected distances and angles are listed in Table 2. As expected, the geometries are broadly similar to those of their dichloride counterparts, with the Ti(1)–Me and Ti(1)–Cp\* distances and other parameters being within the usual ranges. The Ti(1)–Cp\*<sub>cent</sub> (av. 2.07 Å) and Ti–N(1) distances (av. 1.845 Å) are, however, significantly lengthened compared to the dichlorides (corresponding values 2.05 and 1.797 Å, respectively) because of the superior  $\sigma$ -donor ability of Me compared to Cl. The lengthening of the Ti(1)–N(1) distances is accompanied by a shortening of N(1)–C(11) and lengthening of N(2)–C(11), compared to the dichlorides. Apart from these global changes on methylation, there are no significant, systematic structural variations between their bond distances and angles, although as for its dichloride counterpart,  $\text{Cp}^*\text{Ti}\{\text{NC}(\text{Ar}^{\text{NMe}_2})\text{N}^i\text{Pr}_2\}\text{Me}_2$  (**7-Me**) tends towards the shortest Ti(1)–N(1) distance, but not within three standard deviations difference in comparison with the corresponding values for **1-Me** and **6-Me**.

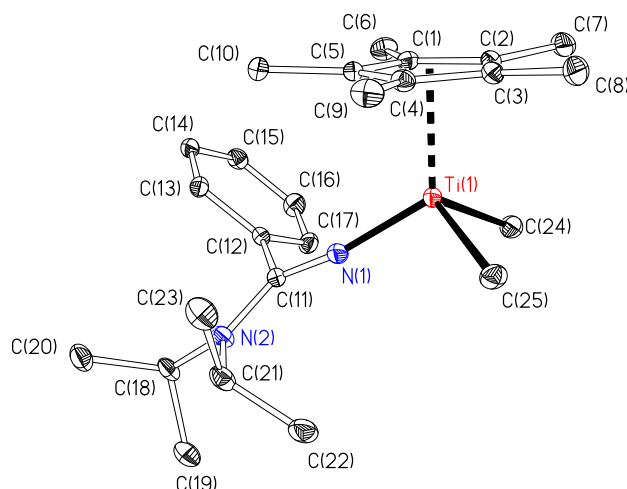


**Figure 4.** Displacement ellipsoid plot of  $\text{Cp}^*\text{Ti}\{\text{NC}(\text{Ph})\text{N}^i\text{Pr}_2\}\text{Me}_2$  (**1-Me**). Displacement ellipsoids are drawn at the 20% probability level and H atoms are omitted.

**Table 2.** Selected bond lengths (Å) and angles (°) for  $\text{Cp}^*\text{Ti}\{\text{NC}(\text{Ph})\text{N}^i\text{Pr}_2\}\text{Me}_2$  (**1-Me**),  $\text{Cp}^*\text{Ti}\{\text{NC}(\text{Ar}^{\text{tBu}})\text{N}^i\text{Pr}_2\}\text{Me}_2$  (**6-Me**) and  $\text{Cp}^*\text{Ti}\{\text{NC}(\text{Ar}^{\text{NMe}_2})\text{N}^i\text{Pr}_2\}\text{Me}_2$  (**7-Me**).  $\text{Cp}^*_{\text{cent}}$  is the computed  $\text{Cp}^*$  ring carbon centroid.

Parameter	<b>1-Me</b>	<b>6-Me</b>	<b>7-Me</b>
Ti(1)- $\text{Cp}^*_{\text{cent}}$	2.07	2.06	2.07
Ti(1)-N(1)	1.845(1)	1.847(2)	1.835(2)
N(1)-C(11)	1.290(2)	1.290(3)	1.297(2)
N(2)-C(11)	1.363(2)	1.357(3)	1.356(2)
C(11)-C(12)	1.502(2)	1.507(4)	1.503(2)
Ti(1)-Me(1)	2.1227(18)	2.108(3)	2.116(2)
Ti(1)-Me(2)	2.1326(19)	2.127(3)	2.1392(18)
$\text{Cp}^*_{\text{cent}}$ -Ti(1)-N(1)	120.8	120.3	119.7
$\text{Cp}^*_{\text{cent}}$ -Ti(1)-Me(1)	113.9	114.1	114.1
$\text{Cp}^*_{\text{cent}}$ -Ti(1)-Me(2)	113.9	113.3	114.4
C(11)-N(1)-Ti(1)	163.00(13)	161.1(2)	163.05(18)

The crystallographically-determined structures of the bimetallic complexes 1,4- $\text{C}_6\text{H}_4\{\text{C}(\text{N}^i\text{Pr}_2)\text{N}\}_2\{\text{Cp}^*\text{TiMe}_2\}_2$  (**2-Me**) and 1,3- $\text{C}_6\text{H}_4\{\text{C}(\text{N}^i\text{Pr}_2)\text{N}\}_2\{\text{Cp}^*\text{TiMe}_2\}$  are shown in Fig 5, and selected bond distances and angles are listed in Table 3. The solid-state structures are consistent with the variable temperature solution NMR studies described above. As expected from the linking

1,4- and 1,3-phenylene linkages there are no close through-space interactions between the metal centers. The metal centers in **2-Me** are related by crystallographic inversion symmetry whereas those of **3-Me** are independent. Comparison of the metric parameters for **2-Me** and **3-Me** with each other or with those of **1-Me** again revealed no significant structural differences.

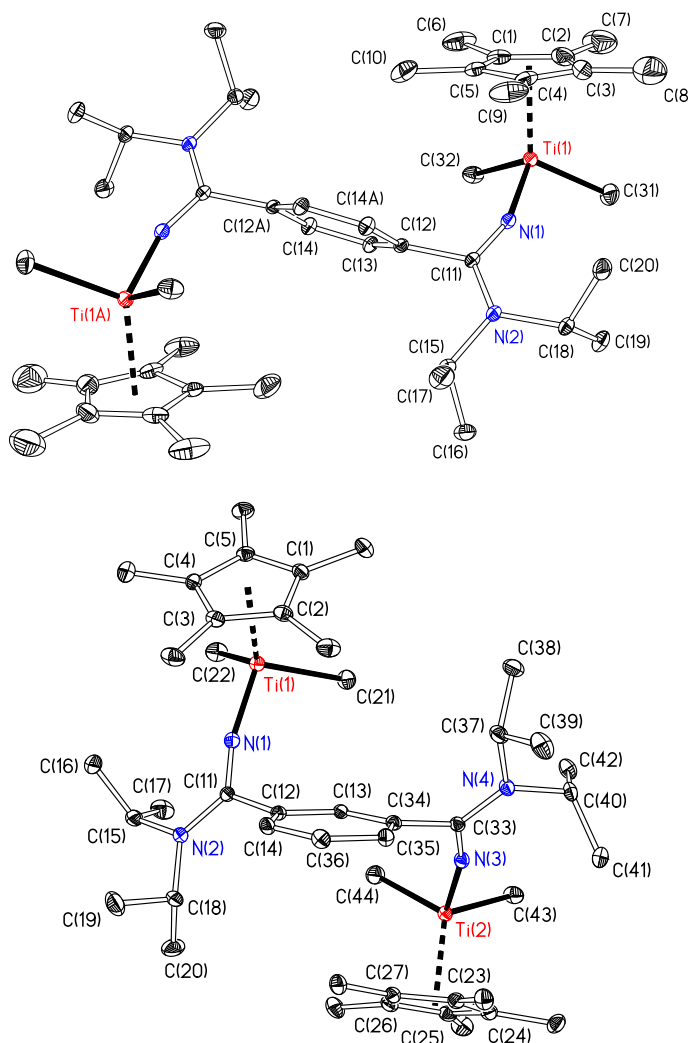


**Figure 5.** Displacement ellipsoid plots of 1,4- $\text{C}_6\text{H}_4\{\text{C}(\text{N}^i\text{Pr}_2)\text{N}\}_2\{\text{Cp}^*\text{TiMe}_2\}_2$  (**2-Me**, top) and 1,3- $\text{C}_6\text{H}_4\{\text{C}(\text{N}^i\text{Pr}_2)\text{N}\}_2\{\text{Cp}^*\text{TiMe}_2\}_2$  (**3-Me**, bottom). Atoms carrying the suffix 'A' are related to their counterparts by the symmetry operator  $2-x, 1-y, 1-z$ .

**Table 3.** Selected bond lengths (Å) and angles (°) for 1,4-C<sub>6</sub>H<sub>4</sub>{C(N<sup>i</sup>Pr<sub>2</sub>)N}<sub>2</sub>{Cp<sup>\*</sup>TiMe<sub>2</sub>}<sub>2</sub> (**2-Me**) and 1,3-C<sub>6</sub>H<sub>4</sub>{C(N<sup>i</sup>Pr<sub>2</sub>)N}<sub>2</sub>{Cp<sup>\*</sup>TiMe<sub>2</sub>}<sub>2</sub> (**3-Me**). Cp<sup>\*</sup><sub>cent</sub> is the computed Cp<sup>\*</sup> ring carbon centroid. For **3-Me** the values in brackets are for the corresponding parameters for Ti(2).

Parameter	<b>2-Me</b>	<b>3-Me</b>	<b>3-Me</b>
Ti(1)-Cp <sup>*</sup> <sub>cent</sub>	2.07	2.07	[2.06]
Ti(1)-N(1)	1.849(2)	1.836(2)	[1.845(2)]
N(1)-C(11)	1.285(3)	1.288(3)	[1.293(3)]
N(2)-C(11)	1.363(2)	1.368(3)	[1.364(3)]
C(11)-C(12)	1.508(3)	1.502(3)	[1.505(3)]
Ti(1)-Me(1)	2.133(3)	2.133(3)	[2.124(3)]
Ti(1)-Me(2)	2.138(3)	2.125(3)	[2.121(3)]
Cp <sup>*</sup> <sub>cent</sub> -Ti(1)-N(1)	119.1	119.6	[120.5]
Cp <sup>*</sup> <sub>cent</sub> -Ti(1)-Me(1)	119.1	113.9	[112.8]
Cp <sup>*</sup> <sub>cent</sub> -Ti(1)-Me(2)	111.0	114.6,	[114.1]
C(11)-N(1)-Ti(1)	159.64(15)	163.05(18)	[163.55(17)]

*Spectroscopic evaluation of the amidinate ligand para-substituents.* <sup>13</sup>C NMR spectroscopy was used as a more sensitive probe of any effects at the titanium centers of the different benzamidinate *para*-substituents in the monometallic complexes **1-Me** and **5-Me** - **7-Me**, and also in the *para*-phenylene-bridged bimetallic **2-Me** by way of comparison. We have also carried out a series of DFT calculations on model compounds (see Fig. 7), including computing the expected <sup>13</sup>C shifts for the Ti-Me groups. The results are summarized in Table 4 and illustrated in Fig. 6.

The data for Cp<sup>\*</sup>Ti{NC(Ar<sup>R</sup>)N<sup>i</sup>Pr<sub>2</sub>}Me<sub>2</sub> show a strong correlation between the Hammett  $\sigma_p$  parameter of the phenyl *para*-substituent (R) and Ti-Me chemical shift, with the more electron-withdrawing -CF<sub>3</sub> group ( $\sigma_p = 0.54$ ) giving the largest  $\delta$  Ti-Me. The agreement between the experimental and computed <sup>13</sup>C values is very good both in terms of absolute chemical shift (relative to SiMe<sub>4</sub>) and the trends in values. The linear fit in Fig. 6 allowed the relationship  $\sigma_p = 1.43\delta(\text{TiMe}) - 14.2$  to be determined. Thus the  $\sigma_p$  value for the -4-C<sub>6</sub>H<sub>4</sub>C(N<sup>i</sup>Pr<sub>2</sub>)NCp<sup>\*</sup>TiMe<sub>2</sub> moiety in **2-Me** can be estimated as 0.15, slightly electron-withdrawing compared to H.

The <sup>13</sup>C NMR data show that although there is no clear structural effect of the varying *para*-substituent that can be determined within the precision of the X-ray diffraction experiments, the

titanium centers are affected to detectable extent. As mentioned, we have probed this further using DFT calculations as discussed in the following section.

**Table 4.** Measured  $^{13}\text{C}$  NMR chemical shifts in  $\text{C}_6\text{D}_6$  for the Ti-Me groups in  $\text{Cp}^*\text{Ti}\{\text{NC}(\text{Ar}^R)\text{N}^i\text{Pr}_2\}\text{Me}_2$  (**1-Me**, **5-Me**–**7-Me** and  $1,4\text{-C}_6\text{H}_4\{\text{C}(\text{N}^i\text{Pr}_2)\text{N}\}_2\{\text{Cp}^*\text{TiMe}_2\}_2$  (**2-Me**) and the DFT computed values for the corresponding model compounds (see Fig. 7) are expressed relative to the computed value for  $\text{SiMe}_4$ .

Compound	$\text{Ar}^R$ <i>p</i> -substituent	Hammett $\sigma_p$ parameter	Measured $\delta \text{TiMe}$ (ppm)	DFT computed $\delta \text{TiMe}$ (ppm)
<b>7-Me</b>	$\text{NMe}_2$	-0.83	46.7	52.3
<b>6-Me</b>	$t\text{Bu}$	-0.20	47.7	53.7
<b>1-Me</b>	H	0.0	47.9	54.3
<b>5-Me</b>	$\text{CF}_3$	0.54	49.0	55.5
<b>2-Me</b>	-	-	48.2	54.7

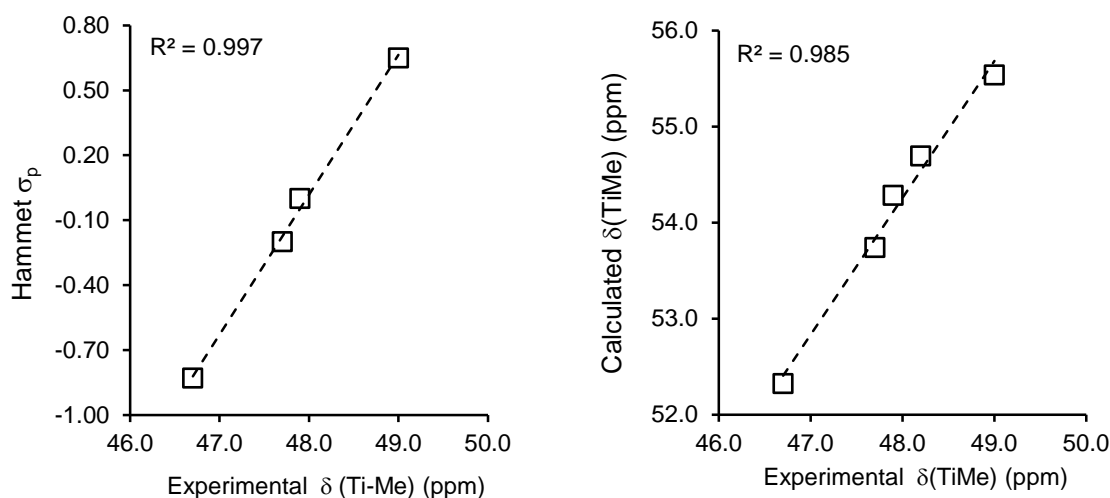


**Figure 6.** (a, left): relationship between *para*-R-group Hammett  $\sigma_p$  parameter and Ti-Me group chemical shift in  $\text{Cp}^*\text{Ti}\{\text{NC}(\text{Ar}^R)\text{N}^i\text{Pr}_2\}\text{Me}_2$ ; (b, right): relationship between DFT computed values for the corresponding model compounds (see Fig. 7) and experimental data for  $\text{Cp}^*\text{Ti}\{\text{NC}(\text{Ar}^R)\text{N}^i\text{Pr}_2\}\text{Me}_2$  and  $1,4\text{-C}_6\text{H}_4\{\text{C}(\text{N}^i\text{Pr}_2)\text{N}\}_2\{\text{Cp}^*\text{TiMe}_2\}_2$  (**2-Me**).

## Computational studies of mono- and bi-metallic amidinate complexes.

To gain a better understanding of the bonding in the new cyclopentadienyl-amidinate complexes described above, computational studies were carried out on a series of model and hypothetical complexes. We used a combination of density functional theory (DFT) at the B3PW91 level, and Bader's quantum theory of atoms-in-molecules (QTAIM<sup>29</sup>). Because we are primarily interested in the electronic structure of the complexes, and the metal centers are similarly sterically encumbered in all of the complexes of interest, we simplified the systems by treating Cp\* as Cp and the amidinate N<sup>i</sup>Pr<sub>2</sub> groups as NMe<sub>2</sub>. To aid the reader, the numbering scheme for the computed complexes follows as closely as possible the one for the real compounds, but with the suffix 'Q' appended (Fig. 7). We also included the ketimide homologue CpTi(NCMe<sub>2</sub>)Me<sub>2</sub> (**8Q**), a model of the real compound Cp\*Ti(NC<sup>t</sup>Bu<sub>2</sub>)Me<sub>2</sub> (**8**).<sup>8a</sup> Table 5 summarizes the main computational results. Details of the calculations and Cartesian coordinates of the structures are provided in the SI.

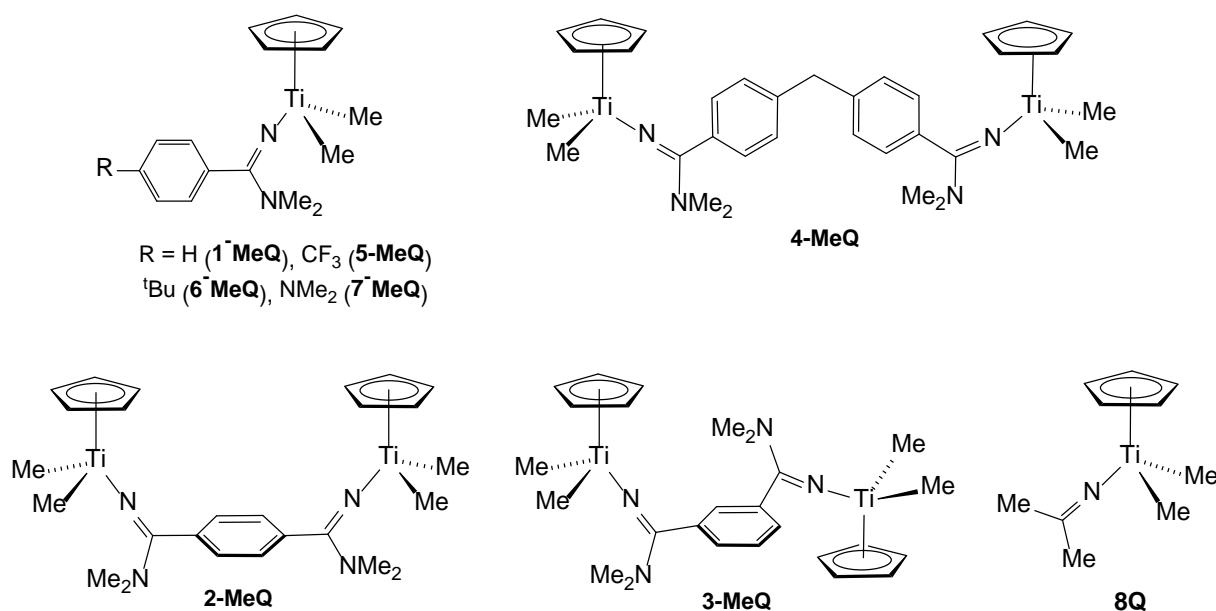


**Figure 7.** Neutral model complexes studied by computational methods.

The geometry-optimised structures of the model compounds are in good agreement with those of the real complexes. A view of the structure of **1-MeQ** is shown in Fig. S5 of the Supporting Information, and Table 5 lists the computed Ti–N distances as a principal geometric parameter. These are systematically shorter than in the real complexes due to the reduced steric bulk, but the underlying trends reproduce those from crystallographic studies as discussed further below. The general electronic structures of CpTi{NC(Ar<sup>R</sup>)NMe<sub>2</sub>}Me<sub>2</sub> and their homologues are in accord with the  $\sigma+2\pi$  Lewis structure depicted in Fig. 3. Molecular orbital analysis reveals two Ti–N  $\pi$ -bonding MOs, with

further orbitals containing the Ti–N  $\sigma$ -bonding interaction. Key MOs for **1-MeQ** are depicted by way of example in Fig. S5 of the Supporting Information.

The nature of the Ti–N interactions in the amidinate and ketimide compounds can be better understood in terms of the interaction between a formal  $[\text{CpTiMe}_2]^+$  fragment and the corresponding  $[\text{NCRR}]^-$  anion. Fig. 8 shows the frontier MOs of the formal amidinate and ketimide anions in **1-MeQ** and **8Q**. The HOMO and HOMO-1 (denoted  $\pi_h$  and  $\pi_v$ ) form the Ti–N  $\pi$ -bonding components, with HOMO-2 giving the  $\sigma$ -bond. In terms of the Lewis structures in Fig. 3, the  $\pi_h$  (lone pair) and  $\sigma$  MOs represent the interactions indicated in the resonance form **A** ( $\sigma+\pi$ ), and additional donation from  $\pi_v$  is the formal second electron pair involved in the resonance form **B** ( $\sigma+2\pi$ ). As is clear from Fig. 8,  $\pi_v$  is in fact the C=N  $\pi$ -bonding component of the amidinate/ketimide moieties. Although  $\pi_v$  overlaps well with the relevant titanium fragment MO, its energy match is poorer than that of  $\pi_h$  which is effectively a N-based 2p AO lone pair. The key role of the amidinate  $-\text{NR}_2$  substituent in enhancing the Ti–N  $\pi$ -bonding interactions (represented in resonance form **B**) arises from the destabilising,  $\pi^*$ -antibonding effect evident in the  $\pi_v$  of  $[\text{NC}(\text{Ph})\text{NMe}_2]^-$  but absent in  $[\text{NCMe}_2]^-$ . This decreases the HOMO/HOMO-1 gap of the anion from 3.356 eV in  $[\text{NCMe}_2]^-$  to 1.527 eV in  $[\text{NC}(\text{Ph})\text{NMe}_2]^-$ , thus making  $\pi_v$  more comparable to  $\pi_h$  (in terms of relative energy) in the amidinate system and the Ti–N  $\pi$ -bonding more cylindrical.

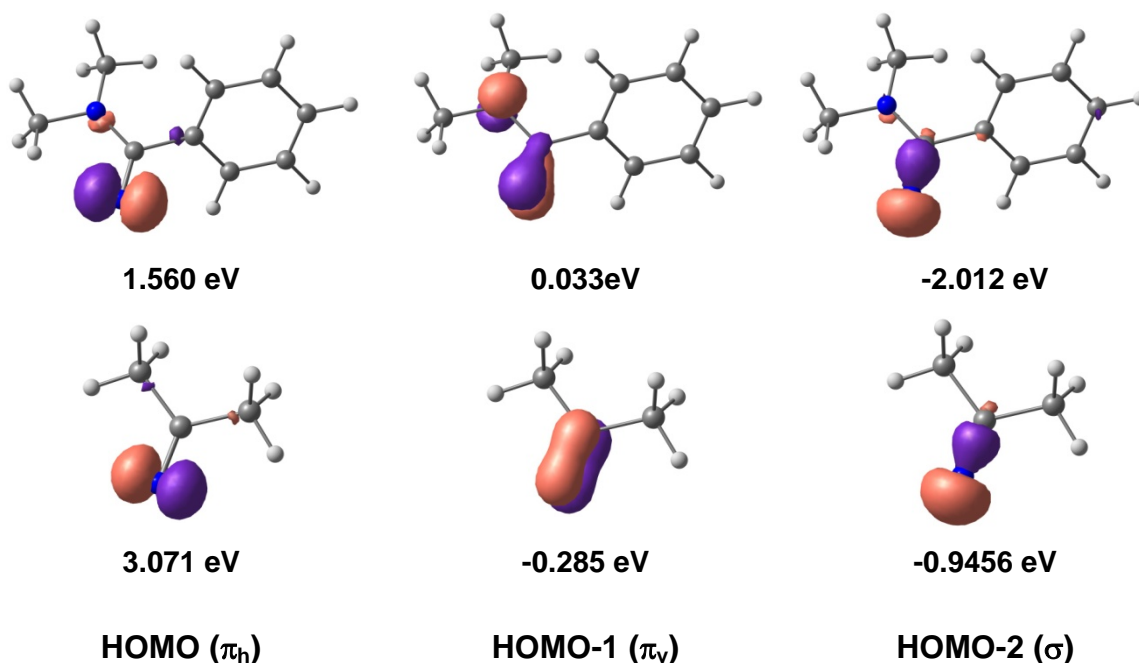


**Figure 8.** Frontier MOs for  $[\text{NC}(\text{Ph})\text{NMe}_2]^-$  (top) and  $[\text{NCMe}_2]^-$  (bottom) computed as spin state singlets in the optimised geometries of **1-MeQ** and **8Q**, respectively. The value for the isosurfaces is 0.052 au.

**Table 5.** Computed parameters for  $\text{CpTi}\{\text{NC}(\text{Ar}^{\text{R}})\text{NMe}_2\}\text{Me}_2$  (**1-MeQ** and **5-MeQ** – **7-MeQ**),  $\text{CpTi}(\text{NCMe}_2)\text{Me}_2$  (**8Q**), 1,4- $\text{C}_6\text{H}_4\{\text{NCNMe}_2\}_2\{\text{CpTiMe}_2\}_2$  (**2-MeQ**), 1,3- $\text{C}_6\text{H}_4\{\text{NCNMe}_2\}_2\{\text{CpTiMe}_2\}_2$  (**3-MeQ**), and  $\text{CH}_2\{1,4\text{-C}_6\text{H}_4\text{-C}(\text{NH})\text{NMe}_2\}_2\{\text{CpTiMe}_2\}_2$  (**4-MeQ**) and the monomethyl cations of the bimetallic species ( $[\mathbf{xQ}]^+$ ). QTAIM data at the Ti–N BCPs are given in atomic units: electron density ( $\rho_{\text{b}}$ ), electron density Laplacian ( $\nabla^2\rho_{\text{b}}$ ), ellipticity ( $\varepsilon$ ), total electronic energy density ( $H_{\text{b}}$ ) and delocalization index ( $\delta(\text{Ti-N})$ ).

Entry	Complex	$\sigma_{\text{p}}$ ( <i>para</i> -R)	Ti-N (Å)	$Q(\text{CpTiMe}_2)$	$\rho_{\text{b}}$ (au)	$\delta(\text{Ti-N})$	$\varepsilon$	$\nabla^2\rho_{\text{b}}$ (au)	$H_{\text{b}}$ (au)
1	<b>7-MeQ</b>	-0.83 (NMe <sub>2</sub> )	1.827	0.413	0.145	0.964	0.214	0.580	-0.051
2	<b>6-MeQ</b>	-0.20 ( <sup>t</sup> Bu)	1.832	0.431	0.143	0.942	0.218	0.572	-0.049
3	<b>1-MeQ</b>	0 (H)	1.833	0.435	0.143	0.937	0.220	0.571	-0.049
4	<b>5-MeQ</b>	0.54 (CF <sub>3</sub> )	1.838	0.456	0.141	0.918	0.226	0.566	-0.047
5	<b>8Q</b>	-	1.856	0.475	0.135	0.892	0.383	0.548	-0.042
8	<b>4-MeQ</b>	-	1.833	0.435	0.143	0.938	0.219	0.571	-0.049
6	<b>2-MeQ</b>	-	1.834	0.443	0.142	0.934	0.230	0.575	-0.048
7	<b>3-MeQ</b>	-	1.835	0.444	0.142	0.930	0.230	0.574	-0.047
9	<b>[2-MeQ]<sup>+</sup></b>	-	1.852	0.507	0.135	0.864	0.238	0.550	-0.042
10	<b>[3-MeQ]<sup>+</sup></b>	-	1.845	0.493	0.137	0.892	0.246	0.563	-0.044
11	<b>[4-MeQ]<sup>+</sup></b>	-	1.837	0.438	0.142	0.927	0.210	0.5644	-0.048



As mentioned, Table 5 lists the computed Ti–N distances as a principal geometric parameter in all the compounds under consideration. For further insight into the Ti–N interactions beyond the general MO analysis we analysed the electron density from the DFT calculations using the QTAIM.<sup>29</sup> The key QTAIM parameters here are (i)  $\rho_b$ , the electron density at the bond critical point (BCP) which can relate to bond strength within a homologous series, and (ii) the delocalization index  $\delta(\text{Ti–N})$ , a measure of the relative bond order within a homologous series. More generally, the positive values for the electron density Laplacian ( $\nabla^2\rho_b$ ) and negative values for the electronic energy density ( $H_b$ ) indicate covalent, donor-acceptor-like interactions between Ti and N. The ellipticity ( $\epsilon$ ) values show that the distribution of electron density at the Ti–N BCPs is not cylindrical, consistent with the MO analysis (non-equivalent  $\pi_h$  and  $\pi_v$ ), and the description of the Ti–N bonding as formally being inbetween forms **A** ( $\sigma + \pi$ ) and **B** ( $\sigma + 2\pi$ ) in Fig 3. By way of example,  $\epsilon = 0$  in  $\text{C}_2\text{H}_2$  ( $\sigma^2\pi^4$ ) but  $> 0$  in  $\text{C}_2\text{H}_4$  ( $\sigma^2\pi^2$ ).  $Q(\text{CpTiMe}_2)$  values are also given in the Table. These are the formal charges on the various CpTiMe<sub>2</sub> fragments (i.e., sum of the QTAIM atomic charges), and are the opposites of the charges on the NCRR' ligand fragments. The values lie in the range *ca.* +0.4 to +0.5, reduced from  $Q(\text{CpTiMe}_2) = +1.0$  for the cations  $[\text{CpTiMe}_2]^+$  due to covalent interactions with the  $[\text{NCRR}']^-$  anions.

The computational results show a small but systematic structural and electronic effect of varying the Ar<sup>R</sup> group *para*-substituent in CpTi{NC(Ar<sup>R</sup>)NMe<sub>2</sub>}Me<sub>2</sub> from R = NMe<sub>2</sub> to CF<sub>3</sub> (entries 1 – 4, Table 5), in accordance with the <sup>13</sup>C NMR trends for the real systems (Fig. 6 and Table 4). The Ti–N distances lengthen from 1.827 to 1.838 Å, accompanied by the expected decrease in  $\rho_b$  and  $\delta(\text{Ti–N})$  and an increase in  $Q(\text{CpTiMe}_2)$ , all indicating reduced N<sub>amidinate</sub>→Ti donation. Fig. 9(a) depicts the linear correlations between computed Ti–N distance and experimental Hammett  $\sigma_p$ ; Fig. 9(b) illustrates the corresponding relationship for  $\delta(\text{Ti–N})$ . Examination of the energies of the  $\sigma$ - and two  $\pi$ -donor MOs for all four  $[\text{NC}(\text{Ar}^R)\text{NMe}_2]^-$  anions show a general stabilization from R = NMe<sub>2</sub> to CF<sub>3</sub>. The computed Ti–N distances for **1-MeQ** (1.833 Å) and **6-MeQ** (1.834 Å) are almost equal, consistent with the crystallographic data for the real systems (1.845(1) and 1.847(2) Å, Table 2). The computed Ti–N distance for **7-MeQ** (1.827 Å) is noticeably shorter, consistent with the shorter bond length in the real system (1.835(2) Å), although the precision in the crystallographic data did not permit a firm conclusion to be drawn within error at the  $\pm 3\sigma$  level.

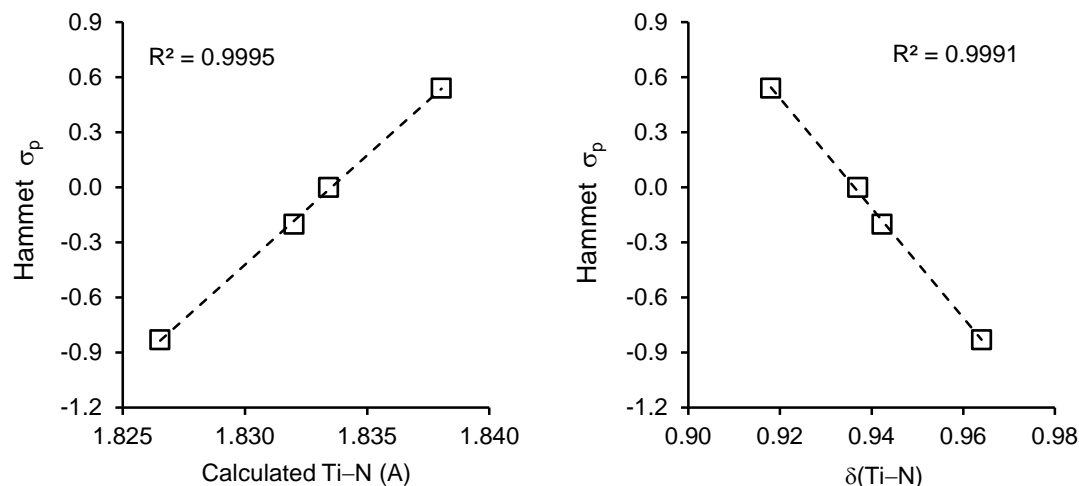


**Figure 9.** Relationship between *para*-R-group Hammett parameter and (a) Ti-N bond distance (left) and (b) delocalization index ( $\delta(\text{Ti-N})$ ) in  $\text{CpTi}\{\text{NC}(\text{Ar}^R)\text{NMe}_2\}\text{Me}_2$  ( $R = \text{NMe}_2$  (**7-MeQ**),  $^t\text{Bu}$  (**6-MeQ**),  $\text{H}$  (**1-MeQ**) or  $\text{CF}_3$  (**5-MeQ**)).

The computational results for the model ketimide **8Q** (entry 5) all indicate that  $\text{N}_{\text{ketimide}} \rightarrow \text{Ti}$  donation is less effective than in the amidinate cases. The longer Ti-N distance for **8Q** (1.856 Å) compared to **1-MeQ** (1.833 Å) is consistent with the experimental dichloride systems  $\text{Cp}^*\text{Ti}\{\text{NC}(\text{Ph})\text{N}^i\text{Pr}_2\}\text{Cl}_2$  (**1-Cl**,  $\text{Ti}(1)-\text{N}(1) = 1.800(3)$  Å) and  $\text{Cp}^*\text{Ti}(\text{NC}^t\text{Bu}_2)\text{Cl}_2$  (**8**,  $\text{Ti-N} = 1.844(7)$  Å) (structural data for the relevant dimethyl compounds are not available).<sup>28</sup> The significantly increased Ti-N bond ellipticity ( $\epsilon$ ) for **8Q** (0.383) is consistent with the reduced role played by the more stabilised  $\pi_v$  MO of  $\text{NCMe}_2$  (*cf.* Fig. 8) in Ti-N  $\pi$ -bonding.

It is informative to compare the computational data for **1-MeQ** with those of the three bimetallic systems (entries 6 – 8). There is no significant difference between the Ti-N distances or any of the QTAIM metrics for **1-MeQ** and **4-MeQ**, the latter of which contains a  $-\text{CH}_2-$  spacer group between the amidinate phenyl rings, suggesting that the methylene group “electronically insulates” the titanium centers from each other. Going from **1-MeQ** and **4-MeQ** to the 1,4- and 1,3-phenylene linked systems **2-MeQ** and **3-MeQ** leads to small but appreciable differences, consistent with the  $^{13}\text{C}$  NMR experiments for **2-MeQ** which suggested that the *para*-titanium-amidinate moieties electronically influence each other by being slightly electron-withdrawing (Table 4). Accordingly, the Ti-N distances and  $Q(\text{CpTiMe}_2)$  charges in **2-MeQ** and **3-MeQ** are increased slightly compared to those in **1-MeQ** and **4-MeQ** while the  $\rho_b$  and  $\delta(\text{Ti-N})$  values are reduced.

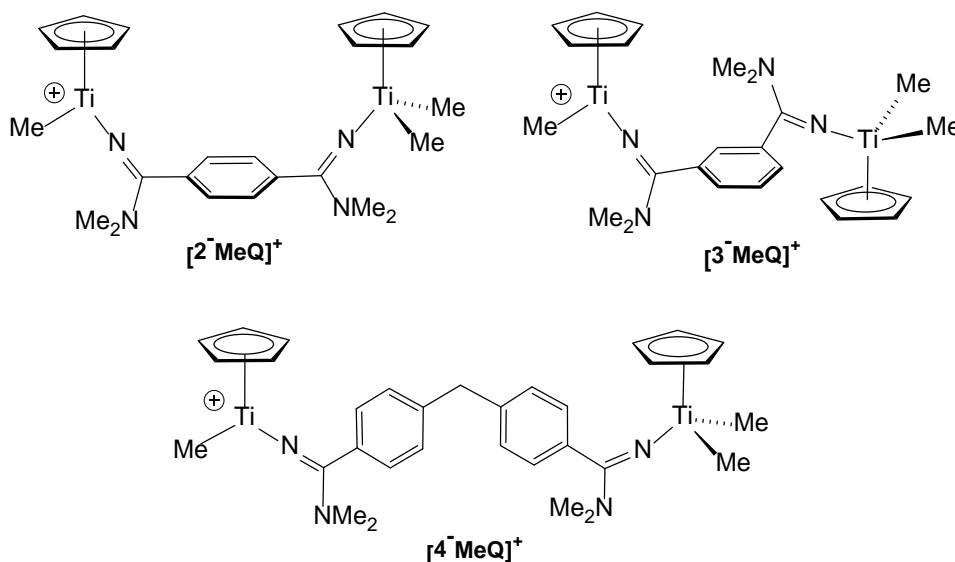


**Figure 10.** Cationic model complexes studied by computational methods.

Under olefin polymerization conditions the mono- and bi-metallic precursors are activated to cationic species of the type  $[\text{CpTi}\{\text{NC}(\text{Ar}^{\text{R}})\text{NMe}_2\}\text{R'}]^+$  ( $\text{R} = \text{H}, \text{NMe}_2, \text{'Bu}$  or  $\text{CF}_3$ ) and  $[(\mu\text{-L})\{\text{C}(\text{N}^i\text{Pr}_2)\text{N}\}_2\{\text{CpTiR'}\}_2]^{2+}$  ( $\text{L} = 1,4\text{-}$  or  $1,3\text{-C}_6\text{H}_4$ ;  $(4\text{-C}_6\text{H}_4)_2\text{CH}_2$ ) where  $\text{R'}$  represents a polymeryl chain. For the monometallic systems the electronic nature of the *para*- $\text{R}$  group does not change on activation, whereas in the bimetallic ones each titanium will now be influenced by a neighboring cationic center. To evaluate the through-bond influence of an adjacent cationic center within the framework of the other model systems studied in Table 5, we optimised and analysed the geometric and electronic structures of the monocationic species illustrated in Fig. 10 (entries 9 – 11 in Table 5).

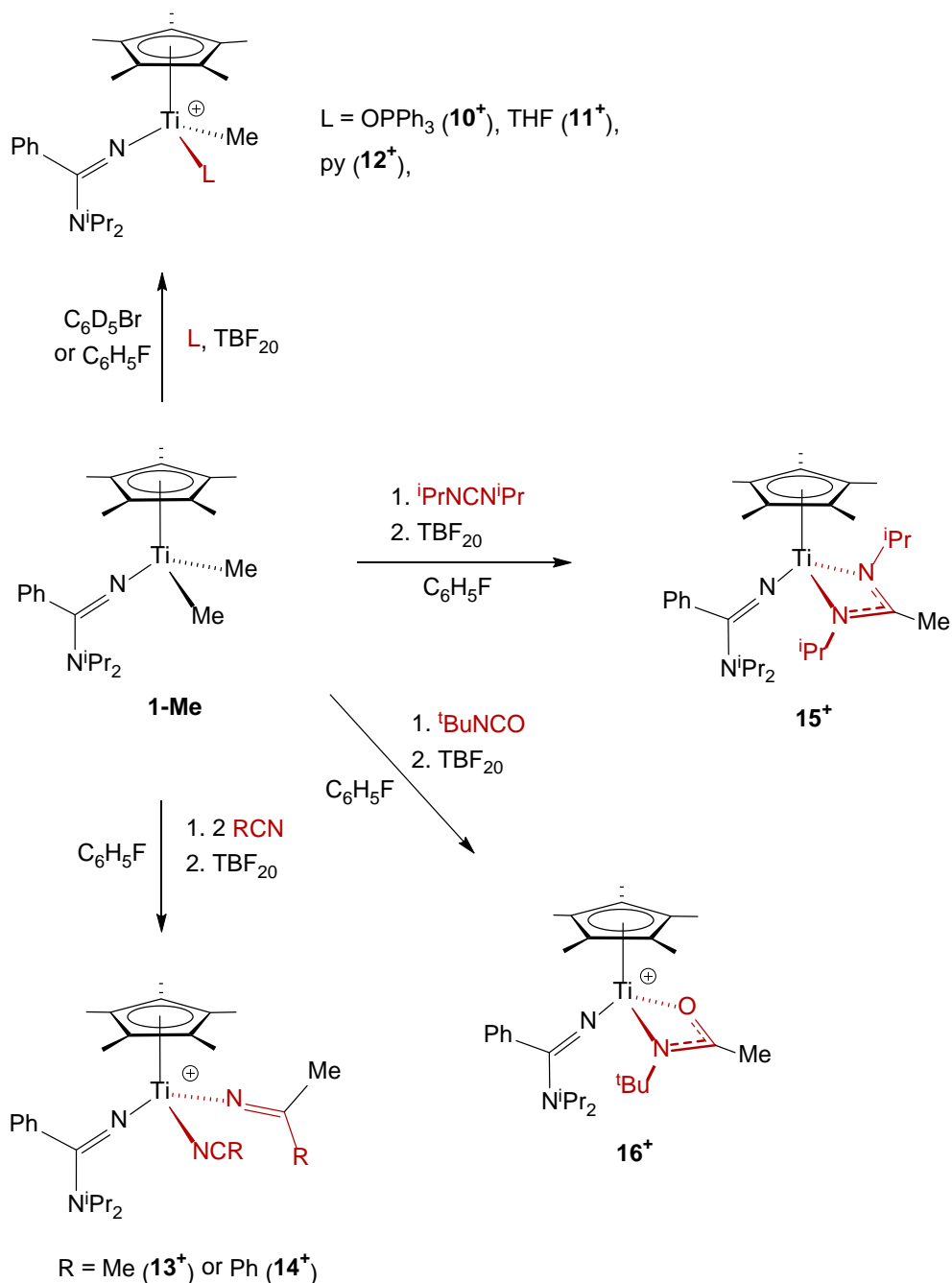
The geometric and QTAIM data for  $[\mathbf{4}\text{-MeQ}]^+$  (methylene spacer, entry 11) indicate a relatively modest effect of the distal cation on the  $\text{-NTiCpMe}_2$  “neutral end”. There is a small increase in  $Q(\text{CpTiMe}_2)$  and  $\text{Ti-N}$  distance, and a decrease in  $\rho_{\text{b}}$  and  $\delta(\text{Ti-N})$  values. By way of comparison we note that the magnitude of the differences between these parameters for  $\mathbf{4}\text{-MeQ}$  and  $[\mathbf{4}\text{-MeQ}]^+$  is less than those between  $\mathbf{1}\text{-MeQ}$  and  $\mathbf{5}\text{-MeQ}$  (*para*- $\text{H}$  vs. *para*- $\text{CF}_3$  groups) again showing the insulating effect of the methylene spacer in this bimetallic system. In contrast,  $[\mathbf{2}\text{-MeQ}]^+$  and  $[\mathbf{3}\text{-MeQ}]^+$  show substantial changes in the key parameters compared to their neutral counterparts. There are significant increases in the  $\text{Ti-N}$  distance and  $Q(\text{CpTiMe}_2)$ , and corresponding decreases in  $\rho_{\text{b}}$  and  $\delta(\text{Ti-N})$ . Electronically, the effect of the distal cationic titanium in  $[\mathbf{2}\text{-MeQ}]^+$  and  $[\mathbf{3}\text{-MeQ}]^+$  is substantially larger than that of a *para*- $\text{CF}_3$  moiety, at least as judged by the DFT results for these model systems. Finally we note that, on going from  $\text{CpTi}\{\text{NC}(\text{Ar}^{\text{NMe}_2})\text{NMe}_2$  ( $\mathbf{7}\text{-Me}$ , entry 1) - having the most electron-releasing *para*-substituents - to  $[\mathbf{2}\text{-MeQ}]^+$  (entry 9) there is a *ca.* 10% decrease in  $\delta(\text{Ti-N})$  and *ca.* 10% increase in  $Q(\text{CpTiMe}_2)$ . The significance of these results with respect to polymerization performance is discussed later on.

## Synthesis and stoichiometric reactions

In order to understand better the activation and reactivity characteristics of representative mono- and bi-metallic amidinate complexes we carried out a number of activation and trapping reactions of cationic derivatives.

*Lewis base adducts and migratory insertion reactions.* The synthesis and reactivity of Group 4 alkyl cations has been extensively investigated, especially with respect to metallocenium systems.<sup>1f, 30</sup> Non-metallocene systems such as phosphinimide- and imido-based systems have also been studied.<sup>6b, 12b, 13, 31</sup> In a preliminary communication<sup>9d</sup> we found that  $\text{Cp}^*\text{Ti}\{\text{NC}(\text{Ar}^{\text{F}2})\text{N}^i\text{Pr}_2\}\text{Me}_2$  (**9-Me**,  $\text{Ar}^{\text{F}2} = 2,6\text{-C}_6\text{H}_3\text{F}_2$ ) cleanly gave the monomethyl cation  $[\text{Cp}^*\text{Ti}\{\text{NC}(\text{Ar}^{\text{F}2})\text{N}^i\text{Pr}_2\}\text{Me}]^+$  (**9**<sup>+</sup>) in  $\text{C}_6\text{D}_5\text{Cl}$  when activated with  $\text{TBF}_{20}$  ( $\text{TBF}_{20} = [\text{CPh}_3][\text{B}(\text{Ar}^{\text{F}5})_4]$ ;  $\text{Ar}^{\text{F}5} = \text{C}_6\text{F}_5$ ). Reaction of **9**<sup>+</sup> with  $\text{OPPh}_3$  gave the Lewis base adduct  $[\text{Cp}^*\text{Ti}\{\text{NC}(\text{Ar}^{\text{F}2})\text{N}^i\text{Pr}_2\}\text{Me}(\text{OPPh}_3)]$ , whereas crystallization of **9-BF<sub>20</sub>** afforded the unusual dimethyl-bridged dication  $[\text{Cp}^*_2\text{Ti}_2\{\text{NC}(\text{Ar}^{\text{F}2})\text{N}^i\text{Pr}_2\}_2(\mu\text{-Me})_2]^{2+}$ . No reactions with other saturated or unsaturated substrates were reported. The reactions of  $\text{Cp}^*\text{Ti}\{\text{NC}(\text{Ph})\text{N}^i\text{Pr}_2\}\text{Me}_2$  (**1-Me**) with Lewis bases, nitriles and *N,N'*-diisopropyl carbodiimide are therefore summarized in Scheme 4. These were chosen as representative substrates based on previous chemistry for Group 4 alkyl cations.

The stoichiometric reaction of **1-Me** with  $\text{TBF}_{20}$  in  $\text{C}_6\text{D}_5\text{Br}$  on the NMR tube scale followed by addition of  $\text{OPPh}_3$  gave immediate and quantitative formation of the Lewis base adduct  $[\text{Cp}^*\text{Ti}\{\text{NC}(\text{Ph})\text{N}^i\text{Pr}_2\}(\text{OPPh}_3)\text{Me}][\text{BF}_{20}]$  (**10-BF<sub>20</sub>**) which was isolated as a yellow powder in 53% yield on scale up. In a similar way, reaction of **1-Me** with  $\text{TBF}_{20}$  in the presence of THF or pyridine gave the corresponding adducts  $[\text{Cp}^*\text{Ti}\{\text{NC}(\text{Ph})\text{N}^i\text{Pr}_2\}\text{Me}(\text{L})][\text{BF}_{20}]$  ( $\text{L} = \text{THF}$  (**11-BF<sub>20</sub>**) or  $\text{py}$  (**12-BF<sub>20</sub>**)) in 70% and 77% isolated yield, respectively. The pyridine adduct **12**<sup>+</sup> seemed to be stable for days at RT and showed no tendency to undergo *ortho*-metallation as was found for the imido-supported cation  $[(\text{Me}_3\text{TACN})\text{Ti}(\text{tBu})\text{Me}]^+$  or several zirconocene alkyl cations.<sup>13, 30c, 32</sup> Reaction of **1-Me** with the borane  $\text{B}(\text{Ar}^{\text{F}5})_3$  (abbreviated as  $\text{BF}_{15}$ ) on the NMR tube scale in  $\text{C}_6\text{D}_5\text{Br}$  followed by addition of THF also formed **11**<sup>+</sup> alongside  $[\text{MeBF}_{15}]^-$  as a non-coordinating anion as discussed further below.<sup>33</sup>

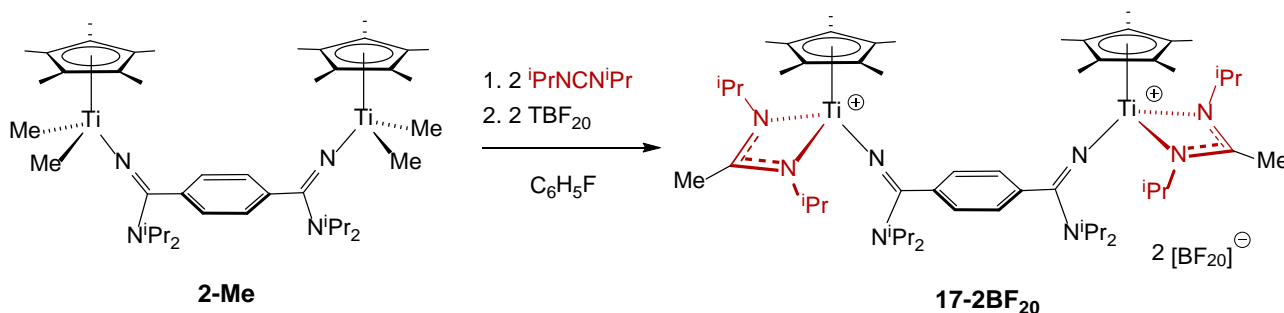


**Scheme 4.** Addition and insertion reactions of *in situ* generated alkyl cations with Lewis bases and unsaturated substrates.  $[\text{TBF}_{20}]^-$  anions and  $\text{MeCPh}_3$  side-products omitted for clarity.

The reaction of the activated titanium complexes with nitriles formed migratory insertion products of the type found previously for metallocenium systems and  $[\text{Ti}(\text{Me}_3\text{TACN})(\text{tBu})\text{Me}]^+$ .<sup>34</sup> Thus reaction of **1-Me** with  $\text{TBF}_{20}$  in the presence of 2 equivalents of  $\text{MeCN}$  gave immediate formation of  $[\text{Cp}^*\text{Ti}\{\text{NC}(\text{Ph})\text{N}^{\text{iPr}}_2\}(\text{NCMe}_2)(\text{NCMe})][\text{BF}_{20}]$  (**13-BF<sub>20</sub>**) which was isolated in 81% yield. The analogous reaction with  $\text{PhCN}$  formed  $[\text{Cp}^*\text{Ti}\{\text{NC}(\text{Ph})\text{N}^{\text{iPr}}_2\}(\text{NCMePh})(\text{NCMe})][\text{BF}_{20}]$  (**14-BF<sub>20</sub>**). The rapid insertion of  $\text{MeCN}$  into the  $\text{Ti-Me}$  bond of **1-Me**<sup>+</sup> is unlike the reaction of  $[\text{Cp}_2\text{TiMe}][\text{BPh}_4]$  which takes 2 weeks to react with this substrate.<sup>34b, 35</sup> Insertion of the nitrile into

the Ti–Me bond as opposed to Ti–N<sub>amidinate</sub> bond of [Cp\*Ti{NC(Ph)N<sup>i</sup>Pr<sub>2</sub>}Me]<sup>+</sup> was established by observed <sup>1</sup>H–<sup>13</sup>C correlations between the migrated methyl group and the Ti–NCMePh carbon of the newly-formed ketimide ligand. Further insertion reactions were carried out with *N,N'*-diisopropylcarbodiimide and *tert*-butylisocyanate as shown in Scheme 4. The reaction of **1-Me** with 1 equiv. of *N,N'*-diisopropylcarbodiimide and TBF<sub>20</sub> gave [Cp\*Ti{NC(Ph)N<sup>i</sup>Pr<sub>2</sub>}{MeC(N<sup>i</sup>Pr)<sub>2</sub>}] [BF<sub>20</sub>] (**15-BF<sub>20</sub>**) in very good isolated yield (77%), as did the corresponding reaction of **1-Me** with TBF<sub>20</sub> and <sup>t</sup>BuNCO, forming [Cp\*Ti{NC(Ph)N<sup>i</sup>Pr<sub>2</sub>}{OC(Me)N<sup>t</sup>Bu}] [BF<sub>20</sub>] (**16-BF<sub>20</sub>**) as a red microcrystalline solid. NMR spectroscopy again confirmed that in both cases the polar heterocumulene substrate had inserted into the Ti–Me bond. Despite repeated attempts we were unable to grow diffraction-quality crystals of an insertion product.

*Activation and trapping of bimetallic complexes.* Corresponding activation reactions with BF<sub>15</sub> and TBF<sub>20</sub> were carried out for **2-Me** as a representative bimetallic analogue of **1-Me**. Reaction with either 1 or 2 equivalents of BF<sub>15</sub> or TBF<sub>20</sub> in C<sub>6</sub>D<sub>5</sub>Br in the absence of added substrate caused a dark oil to form immediately before any NMR data could be recorded. Gratifyingly, however, in the presence of the solubilising *N,N'*-diisopropylcarbodiimide the bis(insertion) product [1,4-C<sub>6</sub>H<sub>4</sub>{C(N<sup>i</sup>Pr<sub>2</sub>)N}<sub>2</sub>{Cp\*Ti{MeC(N<sup>i</sup>Pr)<sub>2</sub>}<sub>2</sub>][BF<sub>20</sub>]<sub>2</sub> (**17-2BF<sub>20</sub>**) was formed quantitatively on the NMR tube scale in the presence of 2 equivalents of both the carbodiimide and TBF<sub>20</sub>. This compound was isolated in 60% yield on scale-up (Eq. 2). The corresponding reaction using 2 equivs of BF<sub>15</sub> formed the same dication on the NMR tube scale along with [MeBF<sub>15</sub>]<sup>−</sup>. The NMR and other data for **17**<sup>2+</sup> are analogous to those for the other insertion products and consistent with the connectivity proposed in Eq. 2. These experiments show that both metal centers in **2** can be activated by borate or borane, and that activation of one metal center does not significantly impede activation (methyl abstraction) at the other metal center.

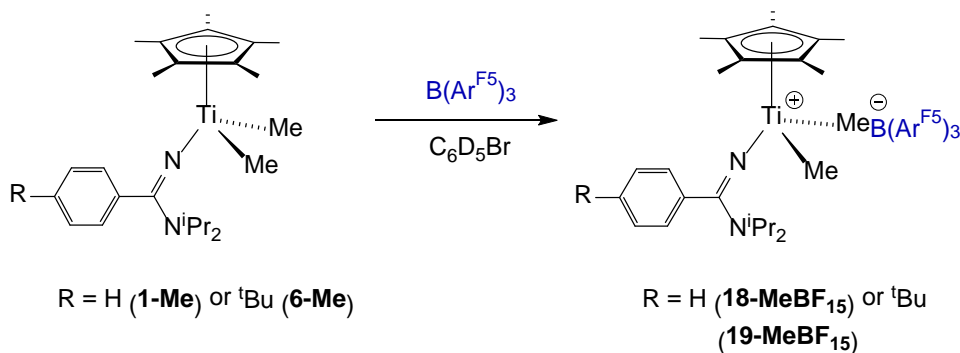


**Equation 2**

*Probe reactions with BF<sub>15</sub>.* The metal centers in **1-Me** and **5-Me** – **7-Me** are influenced by the amidinate *para*-substituents as determined by the experimental <sup>13</sup>C NMR and computational

DFT/QTAIM studies described above. In an attempt to probe this further we set out to measure the  $^1\text{H}$  and  $^{19}\text{F}$  NMR spectra of the  $[\text{Cp}^*\text{Ti}\{\text{NC}(\text{Ar}^{\text{R}})\text{N}^i\text{Pr}_2\}\{\text{MeC}(\text{N}^i\text{Pr})_2\}]^+ / [\text{MeBF}_4]^-$  ion pairs formed on reaction of these five dimethyl compounds with  $\text{BF}_3$  in  $\text{C}_6\text{D}_5\text{Br}$  as a non-reactive/non-donor solvent. Horton *et al.* previously found that the separation ( $\Delta_{m,p}$ ) of the *meta*- and *para*-  $^{19}\text{F}$  chemical shifts in  $[\text{MeBF}_4]^-$  is a probe of the degree of anion association for cationic Group 4 metals.  $\Delta_{m,p}$  values in the range 3 - 6 ppm indicate “coordination” whereas values below 3 ppm indicate “non-coordination”.<sup>33</sup> We hoped that we could use  $\Delta_{m,p}$  as a probe of the electronic properties of the titanium centre in the activated monomethyl cations.

NMR tube scale reaction between **1-Me** and **6-Me** and  $\text{BF}_3$  in  $\text{C}_6\text{D}_5\text{Br}$  quantitatively formed single products identifiable as the ion pairs,  $[\text{Cp}^*\text{Ti}\{\text{NC}(\text{Ph})\text{N}^i\text{Pr}_2\}\text{Me}][\text{MeBF}_4]$  (**18-MeBF<sub>4</sub>**), and  $[\text{Cp}^*\text{Ti}\{\text{NC}(\text{Ar}^{\text{tBu}})\text{N}^i\text{Pr}_2\}\text{Me}][\text{MeBF}_4]$  (**19-MeBF<sub>4</sub>**) (Eq. 3). A  $\Delta_{m,p}$  value of *ca.* 4.7 ppm was measured for both **18-MeBF<sub>4</sub>** and **19-MeBF<sub>4</sub>**. Although these values clearly indicate coordination of  $[\text{MeBF}_4]^-$  they also show that there is no detectable electronic differences between the titanium centers in these cations (consistent with expectation). Addition of 1 equiv. THF to **18-MeBF<sub>4</sub>** formed  $[\text{Cp}^*\text{Ti}\{\text{NC}(\text{Ph})\text{N}^i\text{Pr}_2\}\text{Me}(\text{THF})][\text{MeBF}_4]$  (**11-MeBF<sub>4</sub>**) with a  $\Delta_{m,p}$  value = 2.55 ppm (indicating a non-coordinating  $[\text{MeBF}_4]^-$  anion). Unfortunately, the analogous reactions of **5-Me** or **7-Me** (having the largest differences in  $^{13}\text{C}$  shift for Ti-Me) with  $\text{BF}_3$  immediately resulted in the formation of an insoluble oil. It was not possible, even under very dilute conditions to record NMR data. As check that cations were being formed cleanly in these two cases, carbodiimide insertion complexes of **5-Me** and **7-Me** were synthesised by adding 1 equiv. of *N,N'*-diisopropylcarbodiimide prior to  $\text{BF}_3$ , forming  $[\text{Cp}^*\text{Ti}\{\text{NC}(\text{Ar}^{\text{CF}_3})\}\{\text{MeC}(\text{N}^i\text{Pr})_2\}][\text{MeBF}_4]$  (**20-MeBF<sub>4</sub>**) and  $[\text{Cp}^*\text{Ti}\{\text{NC}(\text{Ar}^{\text{NMe}_2})\}\{\text{MeC}(\text{N}^i\text{Pr})_2\}][\text{MeBF}_4]$  (**21-MeBF<sub>4</sub>**) on the NMR tube scale.



**Equation 3**

## Polymerization studies

We have evaluated the olefin co-polymerization capability of the new mono- and bimetallic titanium dimethyl complexes in conjunction with a trityl borate or a neutral borane as activator. Selected additional experiments were also performed using MAO. In our previous communication we showed that  $\text{Cp}^*\text{Ti}\{\text{NC}(\text{Ar}^{\text{F2}})\text{N}^i\text{Pr}_2\}\text{Me}_2$  (**9-Me**) activated with  $\text{TBF}_{20}$  is a competent catalyst (productivity = *ca.*  $4 \times 10^4 \text{ kg mol}_{\text{Ti}}^{-1} \text{ h}^{-1} \text{ bar}^{-1}$  at  $90^\circ\text{C}$ ;  $M_n = \text{ca. } 200 \text{ kDa}$ ) for the production of an ethylene:propylene (EP) copolymer with an approximately equal  $\text{C}_2:\text{C}_3$  (ethylene:propylene) content (wt%). In our current study we were interested to extend this study of copolymerization performance to EPDM. EPDM (Fig. 11) is a synthetic rubber (elastomer) formed as main-chain-saturated polymer based on the copolymerization of ethylene, propylene and a non-conjugated diene which is incorporated into the chain in typically 2 – 10 wt% quantities. The diene is essential for cross-linking which takes place post-polymerization, typically using sulfur or peroxide reagents. The dienes (Fig. 11) used in this study are ENB (5-ethylidene-2-norbornene) and VNB (5-vinyl-2-norbornene), the more strained internal double bond being incorporated into the main chain.

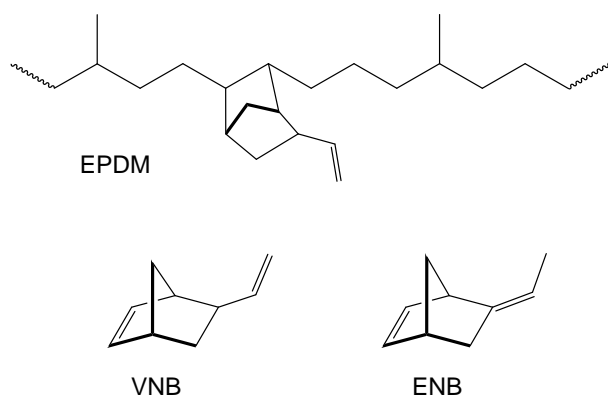


**Figure 11.** Representation of a segment of EPDM and the monomers VNB and ENB

The polymerization results for the monomeric catalysts **1-Me** and **5-Me – 7-Me**, and the bimetallic systems **2-Me – 4-Me** are summarized in Tables 6 and 7. Experiments were performed at  $90^\circ\text{C}$  over a 10 min period (in order to avoid mass transport limitations /drift of monomer concentrations) in 1 L of pentamethylheptane as a high-boiling point hydrocarbon solvent in the presence of non-interacting BHT:TIBA (1:1) scavenger (BHT = 2,6-di*tert*-butyl-4-hydroxytoluene; TIBA = triisobutyl aluminum). A constant monomer stream of  $\text{C}_2:\text{C}_3$  (1:2 molar ratio) was fed through the reactor and a large excess of ENB/VNB relative to the catalyst was introduced into the solution prior to the start of the polymerization experiment. Except where stated otherwise, the ratio of titanium center:borate or borane activator was 1:1. Hydrogen was fed into the reactor vessel along with the gaseous monomers in order to avoid reactor fouling caused by formation of very high molecular weight EPDM.<sup>36</sup> Molecular weights (measured by GPC and expressed relative to PS standards) therefore reflect the



relative rate of propagation and the rates both of chain transfer to hydrogen as well as any  $\beta$ -H elimination since it is known that chain transfer to aluminium with this scavenger system is negligible.<sup>37</sup> The overall wt% C<sub>2</sub>, C<sub>3</sub>, VNB, ENB composition of the EPDMs was determined by quantitative analysis of the isolated polymer films by IR spectroscopy (IR spectroscopy quantifies ENB and VNB according to their pendant double bond). The productivity values are given as kg mol<sub>Ti</sub><sup>-1</sup> h<sup>-1</sup> bar<sup>-1</sup> and calculated per metal center in all cases.

**Table 6.** Polymerization results for Cp\*Ti{NC(4-C<sub>6</sub>H<sub>4</sub>R)N<sup>i</sup>Pr<sub>2</sub>}Me<sub>2</sub> (R = H (**1**), CF<sub>3</sub> (**5-Me**), <sup>t</sup>Bu (**6-Me**) and NMe<sub>2</sub> (**7-Me**) with TBF<sub>20</sub> and BF<sub>15</sub> as activators.<sup>a</sup>

Entry	Precatalyst	Cocatalyst	Productivity <sup>b</sup> (kg mol <sub>Ti</sub> <sup>-1</sup> h <sup>-1</sup> bar <sup>-1</sup> )	C <sub>2</sub> (wt%)	C <sub>3</sub> (wt%)	ENB (wt%)	VNB (wt%)	M <sub>n</sub> (kDa)	M <sub>w</sub> (kDa)	PDI
1	<b>1-Me</b>	TBF <sub>20</sub>	100,630	53.4	45.1	0.96	0.66	266	535	2.0
2	<b>5-Me</b>	TBF <sub>20</sub>	82,800	51.1	47.1	1.10	0.74	214	454	2.1
3	<b>6-Me</b>	TBF <sub>20</sub>	113,660	49.8	48.3	1.16	0.71	259	457	2.2
4	<b>7-Me</b>	TBF <sub>20</sub>	80,330	54.7	43.7	0.98	0.64	210	476	2.3
5	<b>1-Me</b>	BF <sub>15</sub>	76,200	51.7	46.5	1.06	0.76	263	529	2.0
6	<b>5-Me</b>	BF <sub>15</sub>	30,170	49.6	48.6	1.07	0.74	253	547	2.2
7	<b>6-Me</b>	BF <sub>15</sub>	90,510	51.5	46.9	0.99	0.68	220	497	2.3
8	<b>7-Me</b>	BF <sub>15</sub>	53,660	55.2	42.8	1.18	0.82	251	638	2.5

<sup>a</sup> Polymerization conditions: T = 90 °C, pressure = 8 bar, [catalyst] = 0.1 μmol (0.05 μmol for entry 1), scavenger = BHT:TIBA (1:1), [Al]:[M] = 4,500, [B]:[Ti] = 1:1, 10 min reaction time, solvent = pentamethylheptane (1 L), C<sub>3</sub>:C<sub>2</sub> = 400:200 NI h<sup>-1</sup>, H<sub>2</sub> flow = 0.35 NI h<sup>-1</sup>, ENB: 0.7 mL, VNB: 0.7 mL. Polymer molecular weight and molecular weight distributions were determined in 1,2,4 trichlorobenzene against PS standards. Average composition of the polymers were determined using transmission IR spectroscopy on a pressed polymer film. <sup>b</sup> Productivity per mole of transition metal centers.

**Table 7.** Polymerization results for Cp\*Ti{NC(Ph)N<sup>i</sup>Pr<sub>2</sub>}Me<sub>2</sub> (**1**), 1,4-C<sub>6</sub>H<sub>4</sub>{C(N<sup>i</sup>Pr<sub>2</sub>)N}<sub>2</sub>{Cp\*TiMe<sub>2</sub>}<sub>2</sub> (**2-Me**), 1,3-C<sub>6</sub>H<sub>4</sub>{C(N<sup>i</sup>Pr<sub>2</sub>)N}<sub>2</sub>{Cp\*TiMe<sub>2</sub>}<sub>2</sub> (**3-Me**) and CH<sub>2</sub>{1,4-C<sub>6</sub>H<sub>4</sub>-C(N<sup>i</sup>Pr<sub>2</sub>)N}<sub>2</sub>{Cp\*TiMe<sub>2</sub>}<sub>2</sub> (**4-Me**) with TBF<sub>20</sub> and BF<sub>15</sub> as activators.<sup>a</sup>

Entry	Precatalyst	Cocatalyst	Productivity <sup>b</sup> (kg mol <sub>Ti</sub> <sup>-1</sup> h <sup>-1</sup> bar <sup>-1</sup> )	C <sub>2</sub> (wt%)	C <sub>3</sub> (wt%)	ENB (wt%)	VNB (wt%)	M <sub>n</sub> (kDa)	M <sub>w</sub> (kDa)	PDI
1	<b>1-Me</b>	TBF <sub>20</sub>	100,630	53.4	45.1	0.96	0.66	266	535	2.0
2	<b>2-Me</b>	TBF <sub>20</sub>	113,910	43.6	55.3	0.68	0.43	184	399	2.2
3	<b>3-Me</b>	TBF <sub>20</sub>	25,970	45.3	53.7	0.61	0.38	171	374	2.2
4	<b>4-Me</b>	TBF <sub>20</sub>	132,860	50.5	47.8	0.99	0.70	227	483	2.1
5	<b>1-Me</b>	BF <sub>15</sub>	76,200	51.7	46.5	1.06	0.76	263	529	2.0
6	<b>2-Me</b>	BF <sub>15</sub>	41,310	45.4	53.5	0.66	0.45	226	465	2.1
7	<b>3-Me</b>	BF <sub>15</sub>	11,790	45.6	53.4	0.58	0.37	191	406	2.1
8	<b>4-Me</b>	BF <sub>15</sub>	43,370	52.4	46.0	0.99	0.64	218	469	2.2

<sup>a</sup> Polymerization conditions: T = 90 °C, pressure = 8 bar, [catalyst] = 0.1 μmol (0.05 μmol for entries 1,2,6; 0.02 μmol for entry 4), scavenger = BHT:TIBA (1:1), [Al]:[M] = 4,500, [B]:[Ti] = 1:1, 10 min reaction time, solvent = pentamethylheptane (1 L), C<sub>3</sub>:C<sub>2</sub> = 400:200 NI h<sup>-1</sup>, H<sub>2</sub> flow = 0.35 NI h<sup>-1</sup>, ENB: 0.7 mL, VNB: 0.7 mL. Polymer molecular weight and molecular weight distributions were determined in 1,2,4 trichlorobenzene against PS standards. Average composition of the polymers were determined using transmission IR spectroscopy on a pressed polymer film. <sup>b</sup> Productivity per mole of transition metal centers.

*Monometallic catalysts.* Table 6 summarizes the polymerization results for the mononuclear catalysts  $\text{Cp}^*\text{Ti}\{\text{NC}(4\text{-C}_6\text{H}_4\text{R})\text{N}^i\text{Pr}_2\}\text{Me}_2$  ( $\text{R} = \text{H}$  (**1**),  $\text{CF}_3$  (**5-Me**),  $^i\text{Bu}$  (**6-Me**) and  $\text{NMe}_2$  (**7-Me**) with  $\text{TBF}_{20}$  (entries 1 – 4) and  $\text{BF}_{15}$  (entries 5 – 8) as activators. In overall terms, the productivity and polymer composition trends (*cf.* Fig S6 of the Supporting Information) with  $\text{TBF}_{20}$  are the same as with  $\text{BF}_{15}$  showing that the same type of catalyst is formed in each case, and the PDIs ( $M_w/M_n$ ) are consistent with these being well-behaved single site catalysts. The productivities are all systematically lower with  $\text{BF}_{15}$ , in agreement with previous studies of these activators and the poorer coordinating ability of  $[\text{BF}_{20}]^-$  compared to  $[\text{MeBF}_{15}]^-$ .<sup>30b, 38</sup> The general magnitude of productivities for forming EPDM, and the generally comparable  $\text{C}_2:\text{C}_3$  ratios in the polymer, are similar to the results for EP polymerization using **9-Me** activated with  $\text{TBF}_{20}$ .<sup>9d</sup> There is no systematic or significant variation in the amount of each diene (with either activator) incorporated by the different catalysts. VNB is incorporated less readily than ENB because of the differing ring strain in the monomers.

With  $\text{TBF}_{20}$  as the activator, the productivity figures for **5-Me** and **7-Me** (entries 2 and 4) are lower than for **1-Me** and **6-Me** and this is found with  $\text{BF}_{15}$  also (entries 6 and 8). The reasons for this are not obvious: the *para*-phenyl substituents for **5-Me** and **7-Me** ( $\text{CF}_3$  and  $\text{NMe}_2$ ) lie at opposite ends of the range of the  $\sigma_p$  parameters, and all four were shown in NMR tube scale experiments (*vide supra*) to activate quantitatively and cleanly.

In the case of **7-Me** (*para*- $\text{NMe}_2$  group) activated either with  $\text{TBF}_{20}$  or  $\text{BF}_{15}$  there is a small but clear reduction in propylene ( $\text{C}_3$ ) affinity relative to that for ethylene ( $\text{C}_2$ ) (av. wt%  $\text{C}_3$  43.3%) in comparison with the other catalysts. Among the other catalysts with each individual activator there is no other clear trend, but on average, taking both activators into account, the average wt%  $\text{C}_3$  incorporation (47.9%) for **5-Me** (*para*- $\text{CF}_3$  group) is marginally the highest. There are no apparent trends for VNB/ENB content in the various polymers.

*Bimetallic catalysts.* Table 7 summarizes the polymerization results for the bimetallic catalysts  $1,4\text{-C}_6\text{H}_4\{\text{C}(\text{N}^i\text{Pr}_2)\text{N}\}_2\{\text{Cp}^*\text{TiMe}_2\}_2$  (**2-Me**),  $1,4\text{-C}_6\text{H}_4\{\text{C}(\text{N}^i\text{Pr}_2)\text{N}\}_2\{\text{Cp}^*\text{TiMe}_2\}_2$  (**3-Me**) and  $\text{CH}_2\{1,4\text{-C}_6\text{H}_4\text{-C}(\text{N}^i\text{Pr}_2)\text{N}\}_2\{\text{Cp}^*\text{TiMe}_2\}_2$  (**4-Me**), and compares them with the data for the monometallic  $\text{Cp}^*\text{Ti}\{\text{NC}(\text{Ph})\text{N}^i\text{Pr}_2\}\text{Me}_2$  (**1**), all with  $\text{TBF}_{20}$  and  $\text{BF}_{15}$  activation. As found for the monometallic systems (Table 6) there is a general decrease in productivity on going from  $\text{TBF}_{20}$  as activator (entries 1 – 4) to  $\text{BF}_{15}$ . In addition, the relative decrease in productivity is much larger for the bimetallic systems (entries 2 – 4 and 6 – 8, 55 – 67% reduction) than for **1-Me** (entries 1 and 5, 25% decrease). This may indicate a larger increase

in ion-pair binding between the active dication  $[(\mu\text{-L})\{\text{Cp}^*\text{TiR}'\}_2]^{2+}$  ( $\text{R}'$  = polymeryl chain,  $\text{L}$  = bis(amidinate) bridging ligand) and the more polar and “stickier”  $[\text{MeBF}_4]^-$  anions<sup>39</sup> than for the corresponding  $[\text{Cp}^*\text{Ti}\{\text{NC}(\text{Ph})\text{N}^i\text{Pr}_2\}\text{R}']^+$  monocation formed from **1**.

The general trends in productivity and EPDM composition ( $\text{C}_2$ ,  $\text{C}_3$ , diene) and molecular weights (and their associated PDIs) within the series **1** – **4** do not appear to change significantly with activator type. For the purposes of further discussion we will mainly refer to the data sets in entries 1 – 4 with  $\text{TBF}_{20}$ -activation. This also minimises effects arising from different degrees of anion coordination between the mono- and bi-metallic systems.

The productivities for **1-Me** and two bimetallic systems with 1,4-substituted phenyl linkers (**2-Me**:  $\mu\text{-C}_6\text{H}_4$ ) or (**4-Me**:  $\mu\text{-C}_6\text{H}_4\text{-CH}_2\text{-C}_6\text{H}_4$ ) are comparable and substantially larger than for **3-Me** with a  $\mu\text{-1,3-phenylene}$  linker. This may be attributed to a steric effect which is well-precedented in the literature for bimetallic systems as metal centers are brought closer,<sup>14a</sup> and is also evident from the space-filling representations for **2-Me** and **3-Me** given in Fig. S7 of the SI. The molecular weight capability of the bimetallic systems is comparable on average with those of the monometallic ones.

The most noticeable difference between both of the  $\mu\text{-C}_6\text{H}_4$ -linked bimetallics (**2-Me** and **3-Me**) and all the other catalysts studied is the change in polymer composition in terms both of higher  $\text{C}_3$  content relative to  $\text{C}_2$ , and lower ENB/VNB content. This trend is independent of activator type: entries 2 & 3 ( $\text{TBF}_{20}$ ) and 6 & 7 ( $\text{BF}_{15}$ ) in Table 7. This is not due to **2-Me** and **3-Me** simply being bimetallic systems *per se* because **4-Me** does not show this effect. **4-Me** is otherwise analogous to **2-Me** except for the 1,4- $\mu\text{-C}_6\text{H}_4\text{-CH}_2\text{-C}_6\text{H}_4$  linker in place of 1,4- $\mu\text{-C}_6\text{H}_4$ , the intention being to electronically insulate the two metal centers in the active catalysts  $[(\mu\text{-L})\{\text{Cp}^*\text{TiR}'\}_2]^{2+}$ . As an additional check of this result we carried out further EPDM and also ethylene-propylene (EP) polymerization experiments with **1-Me** - **4-Me** with MAO activation (Tables S2 and S3 of the SI). In both cases, **2-Me** and **3-Me** have higher  $\text{C}_3$  affinities than **1-Me** and **4-Me**, and in the case of EPDM a lower diene content.

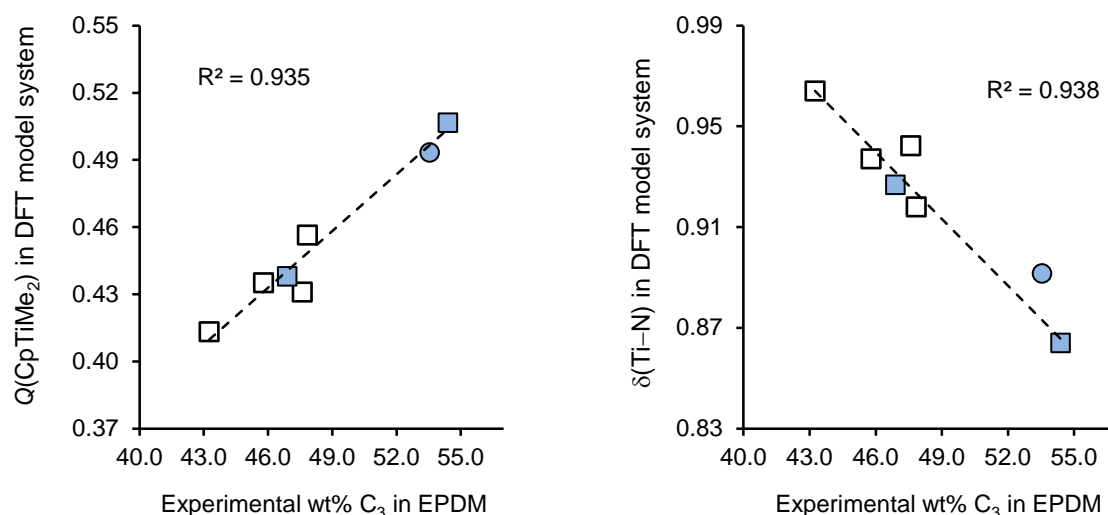


**Figure 12.** Relationship between experimental wt% C<sub>3</sub> incorporation (av. data for TBF<sub>20</sub> and BF<sub>15</sub> activation) and computed (left)  $Q(\text{CpTiMe}_2)$  or (right)  $\delta(\text{Ti-N})$  for the DFT model systems. Key: open squares:  $\text{Cp}^{\text{R}'}\text{Ti}\{\text{NC}(\text{Ar}^{\text{R}})\text{NR}''_2\}\text{Me}_2$ ; filled squares: 1,4- $\text{C}_6\text{H}_4\{\text{C}(\text{NR}''_2)\text{N}\}_2\{\text{Cp}^{\text{R}'}\text{TiMe}_2\}_2$  and  $\text{CH}_2\{1,4\text{-C}_6\text{H}_4\text{-C}(\text{NR}''_2)\text{N}\}_2\{\text{Cp}^{\text{R}'}\text{TiMe}_2\}_2$ ; filled circle: 1,3- $\text{C}_6\text{H}_4\{\text{C}(\text{NR}''_2)\text{N}\}_2\{\text{Cp}^{\text{R}'}\text{TiMe}_2\}_2$ . The linear regression is for the six *para*-substituted systems (open and filled squares). See Fig. S8 and S9 of the SI for the corresponding individual plots for TBF<sub>20</sub> and BF<sub>15</sub> activation.  $\text{Cp}^{\text{R}'} = \text{Cp}$  or  $\text{Cp}^*$ ;  $\text{R}'' = \text{Me}$  or  $i\text{Pr}$ ;  $\text{R} = \text{H}$ ,  $\text{CF}_3$ ,  $t\text{Bu}$  or  $\text{NMe}_2$ .

At first sight the clear change in polymer C<sub>3</sub> uptake in particular with **2-Me** and **3-Me** might be attributed to the sorts of through-space proximity effects described previously in the literature for bimetallic systems.<sup>14</sup> However, we considered that there could alternatively (or additionally) be an electronic explanation. As discussed above in the context of the <sup>13</sup>C NMR and computational studies, the electronic structure at the titanium centers in  $\text{Cp}^*\text{Ti}\{\text{NC}(\text{Ar}^{\text{R}})\text{N}^i\text{Pr}_2\}\text{Me}_2$  are sensitive to the *para*-phenyl substituents in terms of Ti-N interactions (e.g. as judged by the  $\delta(\text{Ti-N})$  values) and fragment charge  $Q(\text{CpTiMe}_2)$ . In addition, when connected *via* either a 1,3- or 1,4- $\text{C}_6\text{H}_4$  bridge (but not a  $\mu\text{-C}_6\text{H}_4\text{-CH}_2\text{-C}_6\text{H}_4$  linker), the charge on one titanium alkyl cation is strongly transmitted to the other one. Fig. 12 explores the potential relationships between C<sub>3</sub> affinity for the real catalyst systems (average data for TBF<sub>20</sub> and BF<sub>15</sub> activation) and the computed  $Q(\text{CpTiMe}_2)$  and  $\delta(\text{Ti-N})$  electronic structure descriptors for model systems. Figs. S8 and S9 of the SI give the corresponding individual plots for TBF<sub>20</sub> and BF<sub>15</sub>.

As can be seen, there is an evident correlation for both the mono- and bi-metallic catalyst systems between the donor ability of the amidinate moiety (as judged by the magnitude of  $Q(\text{CpTiMe}_2)$  and  $\delta(\text{Ti-N})$ ) and  $\text{C}_3$  affinity, with the more strongly donating amidinates (as in **7-Me**) giving the poorest  $\alpha$ -olefin incorporation, and the phenylene-linked bimetallics **2-Me** and **3-Me** having the highest. The bimetallic compound **4-Me** sits among the group of monometallic compounds with moderately-donating amidinate ligands. The factors governing the  $\alpha$ -olefin affinity in Group 4 half-sandwich catalysts are not yet clearly understood or articulated in the literature. It is known that polymerization catalysts of the type  $(\text{L})\text{Ti}(\text{NR})\text{Me}_2$  ( $\text{L} = \text{Me}_3\text{TACN}$  or related  $\text{N}_3$ -donor) with strong  $\sigma+2\pi$  donor imido ligands have no  $\text{C}_3$  affinity at all,<sup>12a, 37a</sup> whereas the titanium constrained geometry catalysts (with  $\sigma + 1\pi$  donor amide ligands) have very high  $\alpha$ -olefin affinity.<sup>3</sup> Cyclopentadienyl-phosphinimide and -ketimide with  $\sigma+2\pi$  donor-like properties have intermediate  $\text{C}_3$  affinities. For example,  $\text{Cp}^*\text{Ti}(\text{NC}^t\text{Bu}_2)\text{Me}_2$  (**8**) produces EP copolymer with 67% wt%  $\text{C}_3$  content under the same conditions used for **1-Me** - **4-Me** (see Table S3 of the SI)

On the basis of the tightly focused series of cyclopentadienyl-amidinate compounds described here we find a correlation based on electronic factors between amidinate ligand donor ability and  $\text{C}_3$  affinity. However, there is no observable correlation between diene (individual or total) content and any of the electronic descriptors within the monometallic systems. One reason for this may be the difficulty in detecting small variations when the baseline wt% incorporation of these monomers is relatively low in any case ( $< 2\%$ ). The sterically more encumbered **2-Me** and **3-Me** systems show an unusually low affinity, with that for **3-Me** being the lowest on average. It seems that the most likely explanation here is that these more sterically-demanding dienes are the most sensitive to the increased steric crowding in **2-Me** and **3-Me** (*cf.* the space-filling representations in Fig. S7 of the SI).

## Summary and conclusions

Straightforward synthesis of the benzamidines  $\text{HNC}(\text{Ar}^{\text{R}})\text{N}^{\text{i}}\text{Pr}_2$  ( $\text{R} = \text{H}$ ,  $\text{CF}_3$ ,  $^t\text{Bu}$  and  $\text{NMe}_2$ ) has allowed us to explore the influence of the *para*-R group on the solid state structures, electronic properties at titanium, and polymerization performance of the corresponding titanium complexes,  $\text{Cp}^*\text{Ti}\{\text{NC}(\text{Ar}^{\text{R}})\text{N}^{\text{i}}\text{Pr}_2\}\text{Me}_2$  ( $\text{R} = \text{H}$  (**1**),  $\text{CF}_3$  (**5-Me**),  $^t\text{Bu}$  (**6-Me**) and  $\text{NMe}_2$  (**7-Me**)).  $^{13}\text{C}$  NMR data together with detailed DFT and QTAIM studies show a small but significant electronic effect at the metal center, with the donor ability of the ligands increasing with decreasing Hammett  $\sigma_{\text{p}}$  parameter in the order  $\text{R} = \text{CF}_3 < \text{H} < ^t\text{Bu} < \text{NMe}_2$ . The amidinate ligands are best thought of as intermediate between 3-electron ( $\sigma+\pi$ ) and 5-electron ( $\sigma+2\pi$ ) donors, and with a larger  $\pi$ -donation contribution than found in the analogous ketimide systems. Use of bis(amidinate) protio-ligands gave access to the corresponding bimetallic derivatives  $1,4\text{-C}_6\text{H}_4\{\text{C}(\text{N}^{\text{i}}\text{Pr}_2)\text{N}\}_2\{\text{Cp}^*\text{TiMe}_2\}_2$  (**2-Me**),  $1,3\text{-C}_6\text{H}_4\{\text{C}(\text{N}^{\text{i}}\text{Pr}_2)\text{N}\}_2\{\text{Cp}^*\text{TiMe}_2\}_2$  (**3-Me**) and  $\text{CH}_2\{1,4\text{-C}_6\text{H}_4\text{-C}(\text{N}^{\text{i}}\text{Pr}_2)\text{N}\}_2\{\text{Cp}^*\text{TiMe}_2\}_2$  (**4-Me**) which were structurally characterised for **2** and **3**. Computational studies found that the metal centers in **2-Me** and **3-Me** responded significantly to changes in charge, whereas those in **4-Me** were much better insulated from each other.

Activation reaction of **1** with  $\text{TBF}_{20}$  led to cationic Lewis base adducts with  $\text{OPPh}_3$ , THF and pyridine, and Ti–Me bond insertion products with the polar substrates MeCN,  $^t\text{BuNCO}$  and  $^i\text{PrNCN}^i\text{Pr}$ . Although nitriles, isocyanates and carbodiimides are susceptible to nucleophilic attack by anionic nitrogen groups, in these amidinate-supported systems the site of reactivity was invariably the Ti–Me group. Reaction of **1** and certain homologues with  $\text{BF}_{15}$  formed soluble inner-sphere ion pairs of the type  $[\text{Cp}^*\text{Ti}\{\text{NC}(\text{Ar}^{\text{R}})\text{N}^{\text{i}}\text{Pr}_2\}\text{Me}][\text{MeBF}_{15}]$  containing coordinating  $[\text{MeBF}_{15}]^-$  anions which were displaced by THF or  $^i\text{PrNCN}^i\text{Pr}$  forming Lewis base adducts or insertion products. Reaction of the bimetallic analogue **2** with 2 equivalents of  $\text{TBF}_{20}$  in the presence of certain trapping reagents showed that both metal centers can be readily activated. All of the monometallic and bimetallic complexes were very active at  $90\text{ }^\circ\text{C}$  for the copolymerization of ethylene, propylene and VNB/ENB for forming EPDM with molecular weights in the range *ca.* 180 – 280 kDa at  $\text{C}_2\text{:C}_3$  ratios between *ca.* 57:43 and 51:49 and around 1% ENB and 0.7% VNB. For the monometallic systems  $\text{Cp}^*\text{Ti}\{\text{NC}(\text{Ar}^{\text{R}})\text{N}^{\text{i}}\text{Pr}_2\}\text{Me}_2$  activated with  $\text{TBF}_{20}$  or  $\text{BF}_{15}$  there was a weak influence of the *para*-R group on the polymer composition such that a slightly lower  $\text{C}_3$  incorporation was found for  $\text{R} = \text{NMe}_2$  and a marginally higher  $\text{C}_3$  content for  $\text{R} = \text{CF}_3$ . There was no effect on



diene incorporation. Analogous results were found for the bimetallic catalyst  $\text{CH}_2\{1,4\text{-C}_6\text{H}_4\text{-C}(\text{N}^i\text{Pr}_2)\text{N}\}_2\{\text{Cp}^*\text{TiMe}_2\}_2$  (**4-Me**). In contrast, for **2-Me** and **3-Me** a more significant increase in  $\text{C}_3$  affinity and decrease in diene content was observed regardless of the activator used (borate/borane and MAO). The variation in  $\text{C}_3$  content across the mono- and bi-metallic catalysts could be correlated with electronic descriptors of the donor ability of the amidinate groups (net charge  $Q(\text{CpTiMe}_2)$  or delocalization index ( $\delta(\text{Ti-N})$ ) in model systems.

The lower diene uptake for **2-Me** and **3-Me** could be attributed to higher steric crowding in the phenylene-bridged systems, indicating the importance of proximity effects in these cases. In addition, although the combined computation and experimental data point to an explanation of increased  $\text{C}_3$  affinity based on electronic factors, the results do not exclude the possibility of additional cooperative effects in **2-Me** and **3-Me** of the types reported for other closely-positioned bimetallic systems.

## Experimental Section

Representative syntheses are given below. Further information is given in the Supporting Information.

**$\text{Cp}^*\text{Ti}\{\text{NC}(\text{Ph})\text{N}^i\text{Pr}_2\}\text{Me}_2$  (**1-Me**).** To a stirring toluene (15 mL) solution of  $\text{Cp}^*\text{Ti}\{\text{NC}(\text{Ph})\text{N}^i\text{Pr}_2\}\text{Cl}_2$  (**1-Cl**) (1 g, 2.2 mmol) was added dropwise MeLi (2.7 mL, 1.6 M in  $\text{Et}_2\text{O}$ , 2.2 mmol) and the resulting solution was stirred for 16 h. The volatiles were then removed *in vacuo* and the yellow solid was then extracted into n-hexanes (50 mL). Concentration of the solution to *ca.* 15 mL and subsequent storage at  $-30\text{ }^\circ\text{C}$  for 24 h resulted in crystallization of the desired product as large yellow crystals which were isolated and dried *in vacuo*. Yield: 0.37 g (40 %).  $^1\text{H}$  NMR (Toluene- $d_8$ , 299.9 MHz, 233 K): 7.23-6.95 (5 H, series of overlapping multiplets,  $\text{C}_6\text{H}_5$ ), 3.60 (1 H, sept,  $\text{CHMe}_2$  *cis* to  $\text{C}_6\text{H}_5$ ,  $^3J = 6$  Hz), 2.91 (1 H, br s,  $\text{CHMe}_2$  *trans* to  $\text{C}_6\text{H}_5$ ), 1.83 (15 H, s,  $\text{C}_5\text{Me}_5$ ), 1.72 (6 H, d,  $\text{CHMe}_2$  *trans* to  $\text{C}_6\text{H}_5$ ,  $^3J = 6$  Hz), 0.64 (6 H, d,  $\text{CHMe}_2$  *cis* to  $\text{C}_6\text{H}_5$ ,  $^3J = 6$  Hz), 0.53 (6 H, s, Me) ppm.  $^{13}\text{C}\{-^1\text{H}\}$  NMR (Toluene- $d_8$ , 233 K): 160.9 ( $\text{NC}(\text{Ph})\text{N}^i\text{Pr}_2$ ), 141.9 (*i*- $\text{C}_6\text{H}_5$ ), 128.1 (*o*- or *m*- $\text{C}_6\text{H}_5$ ), 127.5 (*m*- or *o*- $\text{C}_6\text{H}_5$ ), 126.1 (*p*- $\text{C}_6\text{H}_5$ ), 118.9 ( $\text{C}_5\text{Me}_5$ ), 51.7 ( $\text{CHMe}_2$  *cis* to  $\text{C}_6\text{H}_5$ ), 47.6 (TiMe), 46.5 ( $\text{CHMe}_2$  *trans* to  $\text{C}_6\text{H}_5$ ), 19.9 ( $\text{CHMe}_2$ ), 11.7 ( $\text{C}_5\text{Me}_5$ ) ppm. IR (NaCl plates, Nujol mull,  $\text{cm}^{-1}$ ): 1563 (s), 1506 (w), 1323 (s), 1261 (w), 1132 (w), 1094 (w), 1034 (m), 1023 (m), 886 (m), 782 (s), 696 (m), 666 (m). Anal. found (calcd. for  $\text{C}_{25}\text{H}_{40}\text{N}_2\text{Ti}_1$ ): C, 71.90 (72.10); H, 9.80 (9.68); N, 6.80 (6.73) %. EI-MS  $m/z$ : 203 (5 %,  $[\text{NC}(\text{Ph})\text{N}^i\text{Pr}_2]^+$ ), 135 (5 %,  $[\text{Cp}^*\text{TiMe}_2]^+$ ).

[Cp\*]<sup>+</sup>), 103 (100 %, [NCPh]<sup>+</sup>), 77 (70 %, [Ph]<sup>+</sup>). Single crystals suitable for X-ray diffraction were grown from a pentane solution at – 30 °C.

**1,4-C<sub>6</sub>H<sub>4</sub>{C(N<sup>i</sup>Pr<sub>2</sub>)N}<sub>2</sub>{Cp\*TiMe<sub>2</sub>}<sub>2</sub> (2-Me).** To a stirring toluene (15 mL) solution of 1,4-C<sub>6</sub>H<sub>4</sub>{C(NH)N<sup>i</sup>Pr<sub>2</sub>}<sub>2</sub> (1.01 g, 3.06 mmol) was added a toluene (10 mL) solution of Cp\*TiMe<sub>3</sub> (1.46 g, 6.40 mmol). The brown solution was stirred for 15 h until a precipitate appeared. After filtration the solid was washed with toluene (3 x 15 mL) to produce a yellow solid, which was isolated and dried *in vacuo*. Yield: 1.18 g (51 %) Diffraction quality crystals were grown by slow cooling from a concentrated solution of hot bromobenzene. <sup>1</sup>H NMR (CDCl<sub>3</sub>, 299.9 MHz, 223 K): 7.13 (4H, s, Ar), 3.71 (2H, sept, <sup>3</sup>J = 6.9 Hz, N(CHMe<sub>2</sub>)<sub>2</sub>), 3.51 (2H, br, N(CHMe<sub>2</sub>)<sub>2</sub>), 1.67 (12H, d, <sup>3</sup>J = 6.6 Hz, N(CHMe<sub>2</sub>)<sub>2</sub>), 1.64 (30H, s, C<sub>5</sub>Me<sub>5</sub>), 1.39 (12H, d, <sup>3</sup>J = 6.6 Hz, N(CHMe<sub>2</sub>)<sub>2</sub>), -0.19 (12H, s, TiMe<sub>2</sub>) ppm. <sup>13</sup>C-{<sup>1</sup>H} NMR (CDCl<sub>3</sub>, 75.4 MHz, 223 K): 160.6 (CN(N<sup>i</sup>Pr<sub>2</sub>), 140.2 (Ar C(C(N<sup>i</sup>Pr<sub>2</sub>)N)), 125.5 (Ar CHC(C(NMe<sub>2</sub>)N)), 118.9 (C<sub>5</sub>Me<sub>5</sub>), 51.8 (N(CHMe<sub>2</sub>)<sub>2</sub>), 46.6 (N(CHMe<sub>2</sub>)<sub>2</sub>), 45.9 (TiMe<sub>2</sub>), 20.8 (N(CHMe<sub>2</sub>)<sub>2</sub>), 19.9 (N(CHMe<sub>2</sub>)<sub>2</sub>), 11.3 (C<sub>5</sub>Me<sub>5</sub>) ppm. IR (NaCl plates, Nujol mull, cm<sup>-1</sup>): 1561 (s, C=N), 1321 (m), 1135 (w), 890 (m), 829 (w). EI-MS: *m/z* = 694 (3%, [M – 4Me]<sup>+</sup>). Anal. found (calcd. for C<sub>44</sub>H<sub>74</sub>N<sub>4</sub>Ti<sub>2</sub>): C, 69.85 (70.01); H, 9.68 (9.88); N, 7.57 (7.42) %.

**[Cp\*Ti{NC(N<sup>i</sup>Pr<sub>2</sub>)Ph}(THF)Me][BF<sub>20</sub>] (11-BF<sub>20</sub>).** Cp\*Ti{NC(N<sup>i</sup>Pr<sub>2</sub>)Ph}Me<sub>2</sub> (100 mg, 0.24 mmol) and THF (17 mg, 19 µL, 0.24 mmol) were mixed together in fluorobenzene (10 ml). To this a solution of TBF<sub>20</sub> (221 mg, 0.24 mmol) in fluorobenzene (5 ml) was added. After 30 min pentane (20 ml) was added resulting in the formation of an orange oil. The pentane/fluorobenzene was decanted away and the oil washed further with pentane (10 ml). The remaining solvent was removed *in vacuo* yielding the product as a yellow solid. Yield: 193 mg (70%) <sup>1</sup>H NMR (C<sub>6</sub>D<sub>5</sub>Br, 299.9 MHz, 293 K) 7.20-6.70 (5H, m, C<sub>6</sub>H<sub>5</sub>), 3.47 (1H, br, NCHMe<sub>2</sub>), 3.39 (1H, sept, <sup>3</sup>J = 6.8 Hz, NCHMe<sub>2</sub>), 3.29 (2H, m, OCH<sub>2</sub>), 3.18 (2H, m, OCH<sub>2</sub>), 1.54 (15H, s, C<sub>5</sub>Me<sub>5</sub>), 1.41 (4H, m, OCH<sub>2</sub>CH<sub>2</sub>), 1.23 (1H, d, <sup>3</sup>J = 6.8 Hz, NCHMe<sub>2</sub>), 1.10 (1H, d, <sup>3</sup>J = 6.8 Hz, NCHMe<sub>2</sub>), 0.73 (2H, d, <sup>3</sup>J = 6.6 Hz, NCHMe<sub>2</sub>), 0.51 (3H, s, TiMe) ppm. <sup>13</sup>C-{<sup>1</sup>H} NMR (C<sub>6</sub>D<sub>5</sub>Br, 75.4 MHz, 293 K) 167.6 (NC(N<sup>i</sup>Pr<sub>2</sub>)Ph), 148.9 (br d, <sup>1</sup>J<sub>CF</sub> = 244.4 Hz, *o*-C<sub>6</sub>F<sub>5</sub>), 138.6 (br d, <sup>1</sup>J<sub>CF</sub> = 247.8 Hz, *p*-C<sub>6</sub>F<sub>5</sub>), 137.7 (*i*-C<sub>6</sub>H<sub>5</sub>), 136.8 (br d, <sup>1</sup>J<sub>CF</sub> = 249.0 Hz, *m*-C<sub>6</sub>F<sub>5</sub>), 129.5 (*o*-C<sub>6</sub>H<sub>5</sub>), 128.9 (*m*-C<sub>6</sub>H<sub>5</sub>), 125.6 (C<sub>5</sub>Me<sub>5</sub>), 75.1 (OCH<sub>2</sub>CH<sub>2</sub>), 58.8 (TiMe), 52.3 (NCHMe<sub>2</sub>), 48.5 (NCHMe<sub>2</sub>), 25.2 (OCH<sub>2</sub>CH<sub>2</sub>), 21.5 (NCHMe<sub>2</sub>), 21.0 (NCHMe<sub>2</sub>), 20.5 (NCHMe<sub>2</sub>), 19.8 (NCHMe<sub>2</sub>), 11.7 (C<sub>5</sub>Me<sub>5</sub>) ppm. <sup>19</sup>F NMR (C<sub>6</sub>D<sub>5</sub>Br, 282.1 MHz, 293 K) -131.5 (m, *o*-C<sub>6</sub>F<sub>5</sub>), -161.9 (m, *p*-C<sub>6</sub>F<sub>5</sub>), -165.8 (m, *m*-C<sub>6</sub>F<sub>5</sub>) ppm. <sup>11</sup>B NMR (C<sub>6</sub>D<sub>5</sub>Br, 96.2 MHz, 293 K) -15.9 ppm. IR (NaCl plates, Nujol mull, cm<sup>-1</sup>) 1643 (m), 1595 (w), 1514 (s),

1345 (w), 1261 (w), 1153 (w), 1086 (m), 1023 (w), 980 (s), 891 (w), 844 (w), 789 (w), 775 (w), 756 (w), 668 (w). Anal. Found (calcd. for C<sub>52</sub>H<sub>45</sub>BF<sub>20</sub>N<sub>2</sub>OTi) C, 53.98 (54.19); H, 3.90 (3.94); N, 2.56 (2.43).

**[Cp\*Ti{NC(N<sup>i</sup>Pr)<sub>2</sub>Ph}{MeC(N<sup>i</sup>Pr)<sub>2</sub>}] [BF<sub>20</sub>] (15-BF<sub>20</sub>).** Cp\*Ti{NC(N<sup>i</sup>Pr)<sub>2</sub>Ph}Me<sub>2</sub> (100 mg, 0.24 mmol) and <sup>i</sup>PrNCN<sup>i</sup>Pr (30 mg, 37 μL, 0.24 mmol) were mixed together in fluorobenzene (10 ml). To this a solution of TBF<sub>20</sub> (221 mg, 0.24 mmol) in fluorobenzene (5 ml) was added. After 30 min pentane (20 ml) was added resulting in the formation of a brown solid. The pentane/fluorobenzene was decanted away and the solid washed further with pentane (10 ml). The solid was dried *in vacuo* yielding the product as a brown solid. Yield: 220 mg (77 %). <sup>1</sup>H NMR (CD<sub>2</sub>Cl<sub>2</sub>, 299.9 MHz, 293 K) 7.50-7.20 (5H, m, C<sub>6</sub>H<sub>5</sub>), 4.21 (1H, br, κ<sup>1</sup>-NCHMe<sub>2</sub>), 3.67 (3H, overlapping sept, κ<sup>1</sup> and κ<sup>2</sup>-NCHMe<sub>2</sub>), 2.28 (1H, s, MeC(N<sup>i</sup>Pr)<sub>2</sub>), 2.08 (15H, s, C<sub>5</sub>Me<sub>5</sub>), 1.40 (6H, d, <sup>3</sup>J = 6.9 Hz, κ<sup>1</sup>-NCHMe<sub>2</sub>), 1.12 (6H, d, <sup>3</sup>J = 6.4 Hz, κ<sup>2</sup>-NCHMe<sub>2</sub>), 1.09 (6H, d, <sup>3</sup>J = 6.9 Hz, κ<sup>1</sup>-NCHMe<sub>2</sub>), 0.74 (6H, d, <sup>3</sup>J = 6.4 Hz, κ<sup>2</sup>-NCHMe<sub>2</sub>) ppm. <sup>13</sup>C-{<sup>1</sup>H} NMR (CD<sub>2</sub>Cl<sub>2</sub>, 75.4 MHz, 293K) 170.0 (MeC(N<sup>i</sup>Pr)<sub>2</sub>), 168.5 (NC(N<sup>i</sup>Pr)<sub>2</sub>Ph), 148.7 (br d, <sup>1</sup>J<sub>CF</sub> = 241.7 Hz, *o*-C<sub>6</sub>F<sub>5</sub>), 139.0 (br d, <sup>1</sup>J<sub>CF</sub> = 245.1 Hz, *p*-C<sub>6</sub>F<sub>5</sub>), 137.4 (*i*-C<sub>6</sub>H<sub>5</sub>), 136.9 (br d, <sup>1</sup>J<sub>CF</sub> = 244.4 Hz, *m*-C<sub>6</sub>F<sub>5</sub>), 130.4 (C<sub>5</sub>Me<sub>5</sub>), 130.1 (*o*-C<sub>6</sub>H<sub>5</sub>), 129.4 (*m*-C<sub>6</sub>H<sub>5</sub>), 127.1 (*p*-C<sub>6</sub>H<sub>5</sub>), 51.5 (κ<sup>2</sup>-NCHMe<sub>2</sub>), 49.4 (br, κ<sup>1</sup>-NCHMe<sub>2</sub>), 25.8 (κ<sup>2</sup>-NCHMe<sub>2</sub>), 24.9 (κ<sup>2</sup>-NCHMe<sub>2</sub>), 22.2 (br, κ<sup>1</sup>-NCHMe<sub>2</sub>), 20.7 (κ<sup>1</sup>-NCHMe<sub>2</sub>), 13.9 (MeC(N<sup>i</sup>Pr)<sub>2</sub>), 13.5 (C<sub>5</sub>Me<sub>5</sub>) ppm. <sup>19</sup>F NMR (CD<sub>2</sub>Cl<sub>2</sub>, 282.1 MHz, 293K) -133.0 (m, *o*-C<sub>6</sub>F<sub>5</sub>), -163.8 (m, *p*-C<sub>6</sub>F<sub>5</sub>), -167.6 (m, *m*-C<sub>6</sub>F<sub>5</sub>) ppm. <sup>11</sup>B NMR (CD<sub>2</sub>Cl<sub>2</sub>, 96.2 MHz, 293K) -16.5 ppm. IR (NaCl plates, Nujol mull, cm<sup>-1</sup>) 1643 (m), 1596 (w), 1557 (w), 1540 (m), 1514 (s), 1339 (w), 1311 (w), 1210 (w), 1151 (w), 1085 (s), 1023 (m), 980 (s), 803 (m), 775 (w), 756 (w), 683 (w), 668 (w). Anal. found (calcd. for C<sub>55</sub>H<sub>51</sub>BF<sub>20</sub>N<sub>4</sub>Ti) C, 54.51 (57.74); H, 4.13 (4.26); N, 4.78 (4.64).

**Acknowledgement.** We thank Arlanxeo Netherlands B V for support, and Drs M P Blake, M G Cushion and A D Schwarz and for help with some of the crystallography. We also thank the University of Oxford's Advanced Research Computing facility for access to supercomputer and other resources.

**Supporting Information Available:** General experimental procedures and details of starting materials. Remaining details of the synthesis and characterizing data for new compounds, and polymerization results. Further details of the computational studies, including the computed structures in Cartesian coordinate (.xyz) format. Further details of the crystal structure determinations, including X-ray data collection and processing parameters and further data in

CIF format. This information is available free of charge *via* the internet at <http://pubs.acs.org>. The CCDC codes for the structures in this paper are: CCDC 1498829-1498843

## References

1. (a) Resconi, L.; Chadwick, J. C.; Cavallo, L., Olefin polymerizations with Group 4 metal catalysts. In *Comprehensive Organometallic Chemistry III*, Crabtree, R. H.; Mingos, D. M. P., Eds. Elsevier: Oxford, 2007; Vol. 4; (b) Coates, G. W. *Chem. Rev.* **2000**, *100*, 1223; (c) Ittel, S. D.; Johnson, L. K.; Brookhart, M. *Chem. Rev.* **2000**, *100*, 1169; (d) Baier, M. C.; Zuideveld, M.; Mecking, S. *Angew. Chem. Int. Ed.* **2014**, *53*, 9722; (e) Klosin, J.; Fontaine, P. P.; Figueroa, R. *Acc. Chem. Res.* **2015**, *48*, 2004; (f) Collins, R. A.; Russell, A. F.; Mountford, P. *Appl. Petrochem. Res.* **2015**, *5*, 153.
2. (a) Brintzinger, H. H.; Fischer, D.; Mülhaupt, R.; Rieger, B.; Waymouth, R. M. *Angew. Chem. Int. Ed. Engl.* **1995**, *34*, 1143; (b) Bochmann, M. *J. Chem. Soc., Dalton Trans.* **1996**, 255; (c) Janiak, C., Metallocene catalysts for olefin polymerisation. In *Metallocenes: synthesis, reactivity, applications*, Togni, A.; Halterman, R. L., Eds. Wiley-VCH: New York, 1998; Vol. 2, p 547; (d) Kaminsky, W. *J. Chem. Soc., Dalton Trans.* **1998**, 1413; (e) Resconi, L.; Cavallo, L.; Fait, A.; Piemontesi, F. *Chem. Rev.* **2000**, *100*, 1253.
3. (a) McKnight, A. L.; Waymouth, R. M. *Chem. Rev.* **1998**, *98*, 2587; (b) Braunschweig, H.; Breitling, F. M. *Coord. Chem. Rev.* **2006**, *250*, 2691.
4. (a) Nomura, K. *Dalton Trans.* **2009**, 0, 8811; (b) Nomura, K.; Liu, J. *Dalton Trans.* **2011**, *40*, 7666.
5. (a) Nomura, K.; Naga, N.; Miki, M.; Yanagi, K.; Imai, A. *Organometallics* **1998**, *17*, 2152; (b) Firth, A. V.; Stewart, J. C.; Hoskin, A. J.; Stephan, D. W. *J. Organomet. Chem.* **1999**, *591*, 185; (c) Nomura, K.; Tsubota, M.; Fujiki, M. *Macromolecules* **2003**, *36*, 3797; (d) Kim, T.-J.; Kim, S.-K.; Kim, B.-J.; Son, H.-J.; Hahn, J. S.; Cheong, M.; Mitoraj, M.; Srebro, M.; Piękoś, Ł.; Michalak, A.; Kang, S. O. *Chem. Eur. J.* **2010**, *16*, 5630.
6. (a) Stephan, D. W.; Guérin, F.; Spence, R. E. v. H.; Koch, L.; Gao, X.; Brown, S. J.; Swabey, J. W.; Wang, Q.; Xu, W.; Zoricak, P.; Harrison, D. G. *Organometallics* **1999**, *18*, 2046; (b) Stephan, D. W. *Organometallics* **2005**, *24*, 2548.
7. (a) Kretschmer, W. P.; Dijkhuis, C.; Meetsma, A.; Hessen, B.; Teuben, J. H. *Chem. Commun.* **2002**, 608; (b) Haas, I.; Hübner, C.; Kretschmer, W. P.; Kempe, R. *Chem. Eur. J.* **2013**, *19*, 9132; (c) Wu, X.; Tamm, M. *Coord. Chem. Rev.* **2014**, *260*, 116; (d)

- Nomura, K.; Patamma, S.; Matsuda, H.; Katao, S.; Tsutsumi, K.; Fukuda, H. *RSC Adv.* **2015**, *5*, 64503.
8. (a) Zhang, S.; Piers, W. E.; Gao, X.; Parvez, M. *J. Am. Chem. Soc.* **2000**, *122*, 5499; (b) Nomura, K.; Fujita, K.; Fujiki, M. *J. Mol. Cat. A.* **2004**, *220*, 133; (c) Ferreira, M. J.; Martins, A. M. *Coord. Chem. Rev.* **2006**, *250*, 118.
  9. (a) Ijpeij, E. G.; Zuideveld, M. A.; Arts, H. J.; Van Doremaele, G. H. J. Zwitterionic amidine polyolefin polymerization catalysts. WO2007059881A1, 2007; (b) Ijpeij, E. G.; Windmuller, P. J. H.; Arts, H. J.; Van der Burgt, F.; Van Doremaele, G. H. J.; Zuideveld, M. A. WO/2005/090418 **2005**; (c) Berthoud, A.; Van Doremaele, G. H. J.; Quiroga Norambuena, V.; Scott, R. T. W.; Zuideveld, M. A.; Arts, H. J. **2013**, EP2816050B1; (d) Ijpeij, E. G.; Coussens, B.; Zuideveld, M. A.; van Doremaele, G. H. J.; Mountford, P.; Lutz, M.; Spek, A. L. *Chem. Commun.* **2010**, *46*, 3339.
  10. (a) Britovsek, G. J. P.; Gibson, V. C.; Wass, D. F. *Angew. Chem. Int. Ed.* **1999**, *38*, 428; (b) Kempe, R. *Angew. Chem., Int. Ed. Eng.* **2000**, *39*, 468; (c) Gibson, V. C.; Spitzmesser, S. K. *Chem. Rev.* **2003**, *103*, 283; (d) Redshaw, C.; Tang, Y. *Chem. Soc. Rev.* **2012**, *41*, 4484.
  11. (a) Fujita, T.; Makio, H., 11.20 - Polymerization of Alkenes A2 - Mingos, D. Michael P. In *Comprehensive Organometallic Chemistry III*, Crabtree, R. H., Ed. Elsevier: Oxford, 2007; Vol. 11, pp 691; (b) Makio, H.; Terao, H.; Iwashita, A.; Fujita, T. *Chem. Rev.* **2011**, *111*, 2363; (c) Carpentier, J. F.; Kirillov, E.; Sarazin, Y., Metal Phenolates as Polymerization Catalysts. In *PATAI'S Chemistry of Functional Groups*, Zabicky, J., Ed. John Wiley & Sons, Ltd: 2013.
  12. (a) Bolton, P. D.; Mountford, P. *Adv. Synth. Catal.* **2005**, *347*, 355; (b) Bolton, P. D.; Clot, E.; Cowley, A. R.; Mountford, P. *J. Am. Chem. Soc.* **2006**, *128*, 15005; (c) Bolton, P. D.; Adams, N.; Clot, E.; Cowley, A. R.; Wilson, P. J.; Schroeder, M.; Mountford, P. *Organometallics* **2006**, *25*, 5549; (d) Bigmore, H. R.; Dubberley, S. R.; Kranenburg, M.; Lawrence, S. C.; Sealey, A. J.; Selby, J. D.; Zuideveld, M. A.; Cowley, A. R.; Mountford, P. *Chem. Commun.* **2006**, 436.
  13. Bolton, P. D.; Clot, E.; Adams, N.; Dubberley, S. R.; Cowley, A. R.; Mountford, P. *Organometallics* **2006**, *25*, 2806.
  14. (a) Delferro, M.; Marks, T. J. *Chem. Rev.* **2011**, *111*, 2450; (b) Stürzel, M.; Mihan, S.; Mülhaupt, R. *Chem. Rev.* **2016**, *116*, 1398; (c) McInnis, J. P.; Delferro, M.; Marks, T. J. *Acc. Chem. Res.* **2014**, *47*, 2545.

15. (a) Li, H.; Li, L.; Marks, T. J. *Angew. Chem. Int. Ed.* **2004**, *43*, 4937; (b) Li, H.; Stern, C. L.; Marks, T. J. *Macromolecules* **2005**, *38*, 9015; (c) Noh, S. K.; Kim, S.; Yang, Y.; Lyoo, W. S.; Lee, D.-H. *Eur. Polym. J.* **2004**, *40*, 227.
16. Li, L.; Metz, M. V.; Li, H.; Chen, M.-C.; Marks, T. J.; Liable-Sands, L.; Rheingold, A. L. *J. Am. Chem. Soc.* **2002**, *124*, 12725.
17. (a) Caporaso, L.; Izzo, L.; Sisti, I.; Oliva, L. *Macromolecules* **2002**, *35*, 4866; (b) Salata, M. R.; Marks, T. J. *J. Am. Chem. Soc.* **2008**, *130*, 12; (c) Salata, M. R.; Marks, T. J. *Macromolecules* **2009**, *42*, 1920; (d) Li, H.; Li, L.; Schwartz, D. J.; Metz, M. V.; Marks, T. J.; Liable-Sands, L.; Rheingold, A. L. *J. Am. Chem. Soc.* **2005**, *127*, 14756; (e) Li, H.; Li, L.; Marks, T. J.; Liable-Sands, L.; Rheingold, A. L. *J. Am. Chem. Soc.* **2003**, *125*, 10788.
18. (a) Guo, N.; Stern, C. L.; Marks, T. J. *J. Am. Chem. Soc.* **2008**, *130*, 2246; (b) Guo, N.; Li, L.; Marks, T. J. *J. Am. Chem. Soc.* **2004**, *126*, 6542; (c) Radlauer, M. R.; Agapie, T. *Organometallics* **2014**, *33*, 3247.
19. Motta, A.; Fragalà, I. L.; Marks, T. J. *J. Am. Chem. Soc.* **2009**, *131*, 3974.
20. <http://www.arlanxeo.com>.
21. <http://www.keltan.com/en/home>.
22. Coe, B. J.; Jones, C. J.; McCleverty, J. A.; Bloor, D.; Cross, G. *J. Organomet. Chem.* **1994**, *464*, 225.
23. Hansch, C.; Leo, A.; Taft, R. W. *Chem. Rev.* **1991**, *91*, 165.
24. Fletcher, D. A.; McMeeking, R. F.; Parkin, D. J. *Chem. Inf. Comput. Sci.* **1996**, *36*, 746 (The UK Chemical database Service: CSD updated February 2016).
25. Hagadorn, J. R.; Arnold, J. *Organometallics* **1998**, *17*, 1355.
26. (a) Hazari, N.; Mountford, P. *Acc. Chem. Res.* **2005**, *38*, 839; (b) Mountford, P. *Chem. Commun.* **1997**, 2127.
27. Allen, F. H.; Kennard, O.; Galloy, J. J.; Johnson, O.; Watson, D. G. *Chem. Des. Autom. News* **1993**, *8*, 1 & 31.
28. Dias, A. R.; Duarte, M. T.; Fernandes, A. C.; Fernandes, S.; Marques, M. M.; Martins, A. M.; da Silva, J. F.; Rodrigues, S. S. *J. Organomet. Chem.* **2004**, *689*, 203.
29. Bader, R. F. W., *Atoms in Molecules: A Quantum Theory*. Oxford University Press: Oxford, 1990.
30. (a) Bochmann, M. *Organometallics* **2010**, *29*, 4711; (b) Chen, E. Y.-X.; Marks, T. J. *Chem. Rev.* **2000**, *100*, 1391; (c) Jordan, R. F. *Adv. Organomet. Chem.* **1991**, *32*, 325.

31. Owen, C. T.; Bolton, P. D.; Cowley, A. R.; Mountford, P. *Organometallics* **2007**, *26*, 83.
32. Jordan, R. F.; Taylor, D. F.; Baenziger, N. C. *Organometallics* **1990**, *9*, 1546.
33. Horton, A. D.; de With, J.; van der Linden, A. J.; van de Weg, H. *Organometallics* **1996**, *15*, 2672.
34. (a) Alelyunas, Y. W.; Jordan, R. F.; Echols, S. F.; Borkowsky, S. L.; Bradley, P. K. *Organometallics* **1991**, *10*, 1406; (b) Bochmann, M.; Wilson, L. M.; Hursthouse, M. B.; Motevalli, M. *Organometallics* **1988**, *7*, 1148; (c) Bolton, P. D.; Feliz, M.; Cowley, A. R.; Clot, E.; Mountford, P. *Organometallics* **2008**, *27*, 6096.
35. (a) Bochmann, M.; Wilson, L. M. *J. Chem. Soc., Chem. Commun.* **1986**, 1610; (b) Bochmann, M.; Wilson, L. M.; Hursthouse, M. B.; Short, R. L. *Organometallics* **1987**, *6*, 2556.
36. (a) Ewart, S. W.; Parent, M. A.; Baird, M. C. *J. Polym. Sci., Part A: Polym. Chem.* **1999**, *37*, 4386; (b) Kissin, Y. V.; Mink, R. I.; Nowlin, T. E.; Brandolini, A. J. *J. Polym. Sci., Part A: Polym. Chem.* **1999**, *37*, 4281; (c) Mori, H.; Endo, M.; Terano, M. *J. Mol. Catal. A: Chem.* **1999**, *145*, 211.
37. (a) Adams, N.; Arts, H. J.; Bolton, P. D.; Cowell, D.; Dubberley, S. R.; Friederichs, N.; Grant, C. M.; Kranenburg, M.; Sealey, A. J.; Wang, B.; Wilson, P. J.; Zuideveld, M.; Blake, A. J.; Schroeder, M.; Mountford, P. *Organometallics* **2006**, *25*, 3888; (b) Busico, V.; Cipullo, R.; Cutillo, F.; Friederichs, N.; Ronca, S.; Wang, B. *J. Am. Chem. Soc.* **2003**, *125*, 12402.
38. Yang, X.; Stern, C. L.; Marks, T. J. *J. Am. Chem. Soc.* **1991**, *113*, 3623.
39. Chen, E. Y.-X.; Marks, T. J. *Chem. Rev.* **2000**, *100*, 1391.